Water Selective MFI Zeolite Membranes for Application in the Fischer Tropsch Synthesis

Seyed Alireza Sadat Rezai

Submitted to the University of Cape Town in partial fulfillment of the requirements for the degree of

Masters of Science in Engineering

Department of Chemical Engineering
Catalysis Research Unit
University of Cape Town
Rondebosch 7700
Cape Town
South Africa

June 2005

Abstract

Selective removal of water from the Fischer-Tropsch Synthesis (FTS) during reaction may allow the use of a cobalt catalyst with crystal size <6 nm hence increasing the catalyst activity. Zeolite membranes are a potential route to in-situ water removal due to their chemical and thermal stability under FTS reaction conditions. Zeolite membranes with a low Si/Al ratio are hydrophilic. It has been hypothesised that reducing the Si/Al ratio will result in increased water selectivity and permeance. It is also hypothesised that the separation process can be modelled using the Maxwell-Stefan (MS) formulation.

MFI zeolite membranes were synthesised on α-alumina supports, of varying Si/Al ratio. Two synthesis techniques were used: viz. with and without the assistance of structure directing agents. The membrane physical properties were characterised by SEM and XRD. Membrane quality was evaluated using n-hexane porosimetry. Single gas and mixture separations were carried out. A trans-membrane pressure gradient was applied in single gas measurements. Binary and ternary mixture separations were carried out using a model reaction mixture that approximates FTS conditions. This mixture was fed to a Wicke-Kallenbach cell. The total pressure on both sides of the membrane was equal, with a sweep gas applied to remove the permeate.

Single gas permeation measurements on a blank support shows that viscous and knudsen flow are the dominant transport mechanisms in the support. A single gas permeation model for the zeolite membranes show that viscous and knudsen flow still dominate in pure component measurements. This due to the high flux through the zeolite films. During mixture separations viscous and knudsen flow are negligible as there is no pressure gradient.

Comparing pure component and binary mixture separations the flux of hydrogen decreases by more than two orders of magnitude for the binary case. In the binary system water adsorption results in blockage of pores hence hydrogen permeance is reduced. Binary H_2O/H_2 separation selectivity increases with decreasing

Si/Al ratio. Increasing temperature results in a decrease in this selectivity. Water adsorption decreases with increasing temperature hence hydrogen can permeate faster. With the addition of n-hexane as a third component, permeance of water and hydrogen decrease, however ternary H_2O/H_2 separation selectivity increases.

The Maxwell-Stefan model developed does not predict binary hydrogen permeation well. Permeance is much higher than predicted by the model possibly due to defects. Ternary hydrogen permeance is however more accurately predicted. Water and n-hexane permeance are predicted well by the model.

Acknowledgements

Firstly I am grateful to my supervisor, A/Prof Klaus Möller for his help, guidance, and willingness to listen to my arguments even when it was clear I was wrong, but most of all for letting me have so much of his time. Thank you Klaus! Also a big thanks to my supervisors Prof Jonas Hedlund and Dr Fredrik Jareman at the University of Luleå during my time in Sweden, for their contribution to this work and guidance with some important experimental work. A special thanks to Fredrik for all his amazing ideas for experiments and especially with sorting out broken apparatus :) I would have been so lost without you!

Prof Eric van Steen and Dr Michael Claeys for helping me with the finer details of Fischer-Tropsch Synthesis and catalyst deactivation.

Dr Warwick Duncan our network supervisor for sorting out my laptop issues so often, I don't know what I will do when I leave.

Charlotte Andersson and Olov Öhrman in Luleå for helping and teaching me all the experimental stuff. I would also like to thank all the postgrads in the department for listening to what I had to say and giving me their opinion and input into my work and keeping me company! Thanks to Charles, Chris, Sam, Lebo, Tim, Simon, Itai, Jason, Renate, and Velapi. A special thanks to Jako for SW help! Good luck to you all.

The NRF and SIDA for the financial support of this work and my trip to Sweden, it's a beautiful country :)

Last, but most important of all, thank you to my parents, Saied and Behdokht, for the great support throughout the years, I wouldn't be here without you. A very special thanks to a special person in my life, my girlfriend, Lena for being so patient with me and giving so much time while she was visiting me. Thanks for waiting for me by my window so patiently.

Contents

List of Figures

List of Tables

Nomenclature

Roman Letters

b	Langmuir adsorption coefficient	Pa^{-1}
B	Sum of kundsen and viscous diffusivities	$m^2.s^{-1}$
B_0	Permeability coefficient	m^2
C_i	Concentration of species i	mol. m^{-3}
C_t	Total concentration	mol. m^{-3}
E_a^{sur}	Surface diffusion activation energy	$J.mol^{-1}$
f_i	Pure component fugacity of species i	Pa
$\overline{f_i}$	Mixture component fugacity of species i	Pa
F_i	Flowrate of species i	$ml.min^{-1}$
J_i	Flux of species i	$mol.m^2.s^{-1}$
k	FTS rate constant	$mol^{-1}.s.g.Pa^{3/2}$
K^o	Adsorption coefficient at reference temperature	$mol.g^{-1}$
K_0	Knudsen flow parameter	-
M_i	Molecular mass of species i	$g.mol^{-1}$
N_i	Flux of species i	$ml.min^{-1}$
p_i	Partial pressure of species i	Pa
$\overline{P}$	Average pressure across membrane	Pa
q_i	amount of adsorbed species i	$mol.g^{-1}$
$q_{i,sat}$	saturation amount of adsorbed species i	$mol.g^{-1}$
r_i	Rate of reaction of species i	$mol.s^{-1}$
r_p	Pore radius	m
R	Gas constant	$J.mol^{-1}.K^{-1}$
T	Temperature	K / °C
x_i	Molar fraction of species i	-
$\overline{x_i}$	Average molar fraction of species i	-

Greek Letters

α_{ij}^{ideal}	Ideal selectivity between species i and j	-
$\alpha_{ij}^{k,ideal}$	Ideal knudsen selectivity between species i and j	-
α_{ij}	Separation selectivity between species i and j	-
α'_{ij}	Alternate separation selectivity of species i and j	-
γ_i	Activity coefficent of species i	-
δ	Zeolite film thickness	m
δ_{ij}	Kronecker delta	-
ΔH^{ads}	Heat of adsorption	J.mol^{-1}
ΔH^{rxn}	Heat of reaction	J.mol^{-1}
ΔP_i	Partial pressure difference of species i	Pa
Δx_i	Change in compostion of species i	-
Γ	Thermodynamic correction factor	-
μ_i	Chemical potential of species i	J.mol^{-1}
ν_i	Viscosity of species i	Pa.s
$\nu_{i,0}$	Viscosity of species i at reference temperature	Pa.s
σ_i	Molecular radius of species i	Å
π_i	Permeance of species i	mol.m^2.s^{-1}.Pa^{-1}
ρ	Density	kg.m^{-3}
θ_i	Surface coverage of species i	-
Θ_i	Molecular loading of species i	mole/unit cell
$\Theta_{i,sat}$	Saturation molecular loading of species i	mole/unit cell

Latin Letters

$Đ_i$	Maxwell-Stefan diffusivity of species i in zeolite	m^2.s^{-1}
$Đ_{ij}$	Maxwell-Stefan diffusivity interaction of species i and j	m^2.s^{-1}
$Đ^o$	Diffusivity at reference temperature	m^2.s^{-1}
$Đ_{eff,i}$	Effective diffusivity of species i	m^2.s^{-1}
$Đ_{k,i}$	Knudsen diffusivity of species i	m^2.s^{-1}
$Đ_{v,i}$	Viscous diffusivity of species i	m^2.s^{-1}

Part I

Introduction and Literature review

Chapter 1

Introduction

This chapter will give a brief background to the Fischer-Tropsch Synthesis. It will outline the main objectives of the project. Also the scope and limitations of the project will be discussed.

1.1 Background

The catalysed polymerisation of carbon monoxide with hydrogen to form long chain hydrocarbons, mainly olefins and paraffins and water as a co-product, referred to as the Fischer Tropsch Synthesis (FTS) is industrially very important in South Africa. The reaction may be catalysed with a wide range of catalysts including iron, nickel, cobalt and ruthenium. However, industrially the reaction is catalysed by iron or cobalt. The overall reaction can be represented as:

$$CO + 2H_2 \rightarrow \frac{1}{n}(CH_2)_n + H_2O \qquad \Delta H^{rxn} = -160 \text{ KJ/mol} \qquad (1.1)$$

This reaction is exothermic and as a result industrially the reaction can be carried out in tubular fixed bed reactors with cooling, slurry reactors or fluidized bed reactor with cooling coils which have improved heat transfer. The iron catalyst produces a high yield of α-olefins and also some oxygenates, whereas the cobalt catalyst produces mainly paraffins. The reaction is run at temperatures ranging from 180-240°C (low temperature FTS) and 320-360°C (high temperature FTS) and pressure ranging from 20-40 bar. The cobalt catalyst is 170 times more expensive than the iron catalyst, and for this reason, as well as practical reasons it is supported. The support used is usually Al_2O_3 or SiO_2.

The FTS catalyst undergoes deactivation. It will be shown further on in the

literature review that water has been suggested to cause the deactivation by acting as an oxidizing agent. It also contributes to sintering of the supported catalyst. Therefore, by selectively removing water from the reaction mixture as it is formed, this deactivation may be minimized.

To achieve this selective separation of water in-situ from a continuous process, membrane reactors may be used. Ceramic and glass membranes can not achieve the separation required as they are not selective for the given reaction mixture. There is a large range of polymeric membranes for water desalination, but these membranes have low thermal, chemical and mechanical stability and cannot withstand the harsh reaction conditions of the FTS. Within the last two decades supported porous inorganic oxides have been synthesised that can withstand these conditions, making these ideal candidates for water separation.

1.2 Objectives

The objectives of this project are threefold, they include:

- the synthesis of supported zeolite membranes and characterization of their physical and transport properties,
- an investigation into the application of these membranes for the in-situ removal of water from FTS by performing permeation experiments using model reaction mixtures, and
- derivation of a practical model that will describe the separation of species in the reaction mixture.

Focus of the work will be on investigating H_2O/H_2 selectivity that can be achieved at the given reaction temperatures, the effect of n-hexane, and the water permance as this is essential to have a membrane with a surface area that allows practical application. The major aspects that will be investigated are:

- effect of hydrophilicity of the zeolite on the selectivity of the membranes, and
- effect of competitive adsorption on selectivity.

1.3 Scope and limitations

The scope of this work is to be limited to a model reaction mixture rather than running the actual catalysed reaction. Due to experimental limitations carbon-monoxide will not be introduced. Further more the model reaction will only contain one hydrocarbon rather than the entire spectrum of possible FTS product.

The range of zeolites that may be applied as membranes in FTS are limited. There are currently 161 known zeolite structures, however to date only a handful have successfully been synthesized as continuous membranes and of these only few can synthesised with consistency and quality.

Chapter 2

Literature review

Due to the scarcity of literature, motivation for the project will be two-fold. Initially, advantages of the use of membrane reactors in FTS will be demonstrated by reviewing work already done on the effects of water partial pressure and crystal size on the rate of reaction. Thereafter, synthesis and characterization of zeolite membranes will be reviewed. Furthermore, factors affecting membrane performance, namely permeance and selectivity, will be discussed and some examples for the use of zeolite membranes in water separations will be given. The dominant permeation mechanisms in membranes and typical modelling methods will also be shown. Finally, a summary will be drawn, and from this a hypothesis and key questions for the project will be given.

2.1 Membrane reactors for Fischer Tropsch Synthesis

Although the project does not actually deal with the FTS reaction, nor a model reaction mixture that describes the FTS well, the following sections are essential to the motivation of the project. Membrane reactors are most commonly applied to shift an equilibrium in the desired direction. This is not the case here, the desired outcome is rather improved activity of the catalyst as will be shown in the following sections.

2.1.1 Rate of Fischer Tropsch Synthesis

There are numerous equations in literature that attempt to describe the rate of FTS; however most of these are empirical. Van Steen and Schulz (1999) suggested a set of elementary reactions (see Appendix A) that account for the irreversibility and the

polymerisation characteristics of FTS. They make various assumptions including:

- application of Langmuir-Hinshelwood kinetics,
- equilibrium between surface species and the gas phase species,
- each species only occupies a single active site,
- species occupy the same geometric space, and
- under reaction conditions the surface is mainly covered with surface carbon.

From these, the rate equation for CO consumption is derived as a function of partial pressures of water, hydrogen and carbon monoxide, equation 2.1:

$$-r_{CO} = \frac{kK' \frac{p_{H_2}^{\frac{3}{2}} \cdot p_{CO}}{p_{H_2O}}}{\left(1 + K'' \frac{p_{H_2} \cdot p_{CO}}{p_{H_2O}}\right)^2} \tag{2.1}$$

2.1.2 Effect of water and crystal size

It has been reported that if water is co-fed with the reactants, thereby increasing the partial pressure of water, there is a marked increase in the observed CO conversion. There is also an increase in the C_{5+} selectivity (Krishnamoorthy *et al.*, 2002), which are both desired outcomes. However, Van Berge *et al.* (2000) and Jacobs *et al.* (2002) have carried out studies on the deactivation of the Co catalyst. They reported that increasing the water partial pressure can cause severe deactivation of the catalyst. They suggest catalyst oxidation by water as a mechanism for deactivation. Thermodynamic considerations (Appendix B) show that the bulk oxidation reactions are not favoured under typical FTS conditions. However, Van Berge *et al.* (2000) suggest that for cobalt supported on Al_2O_3, support-cobalt interactions is a possible route to the oxidation. Van Berge *et al.* (2000) indicate that the aluminium-cobalt oxide might be formed as a result of consecutive reaction pathways which maybe more kinetically preferred. Jacobs *et al.* (2003) have observed these aluminium-cobalt oxides by spectroscopy techniques. As the catalyst crystal size becomes smaller the support-cobalt interaction increases due to the higher surface area and surface energy of the crystals.

Figure 2.1 illustrates this effect. Iglesia (1997) has stated that for stable synthesis of the FTS, crystals with a diameter greater than 6nm are required. If dispersion is increased by decreasing the crystal size for a catalyst, instead of a net increase

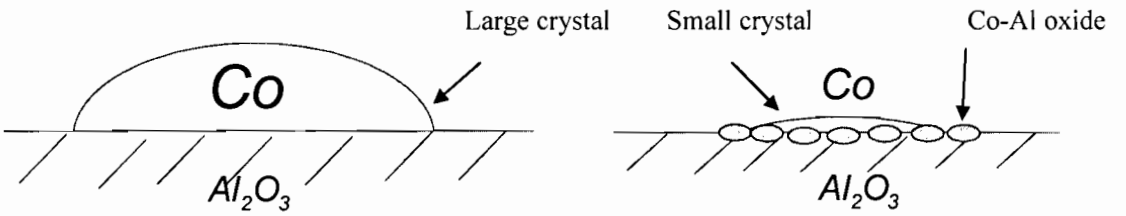

Figure 2.1: The effect of crystal size on the oxidation of cobalt supported on alumina.

in the rate of reaction there is a decrease, as cobalt crystals have a size distribution and any fresh crystals with a diameter less than 6 nm will be deactivated. Figure 2.2 shows the rate of reaction based on equation 2.1. Four scenarios have been modelled:

- CSTR-1 reactor with average catalyst crystal size of 8 nm,
- CSTR-2 reactor with average catalyst crystal size of 4 nm,
- MR-1 (membrane reactor) with average catalyst crystal size of 8 nm, and
- MR-2 with average catalyst crystal size of 4 nm.

It is assumed that the membrane reactor is capable of removing 75% of water produced, a reaction co-product. It can be seen that removal of water allows using crystals with a diameter smaller than 6 nm, hence doubling the activity of the catalyst as crystal size has been reduced. With the removal of water, the decrease in crystal size is possible since the oxidation of these has been assumed to be negligible. It must be noted that there has been no literature found for the optimum amount of water for the FTS catalyst. Hence it is highly beneficial to remove water in-situ from the FTS.

2.2 Zeolite membranes

Membranes may be generally defined as *a permeable barrier between two phases.* This definition holds for a large range of membranes including glasses, metal, ceramics, polymeric, biological and porous membranes. Figure 2.3 represents one such type of membrane, an exotic hollow fibre membrane synthesised on carbon nano-tubes. There are two main categories of membranes: organic and inorganic.

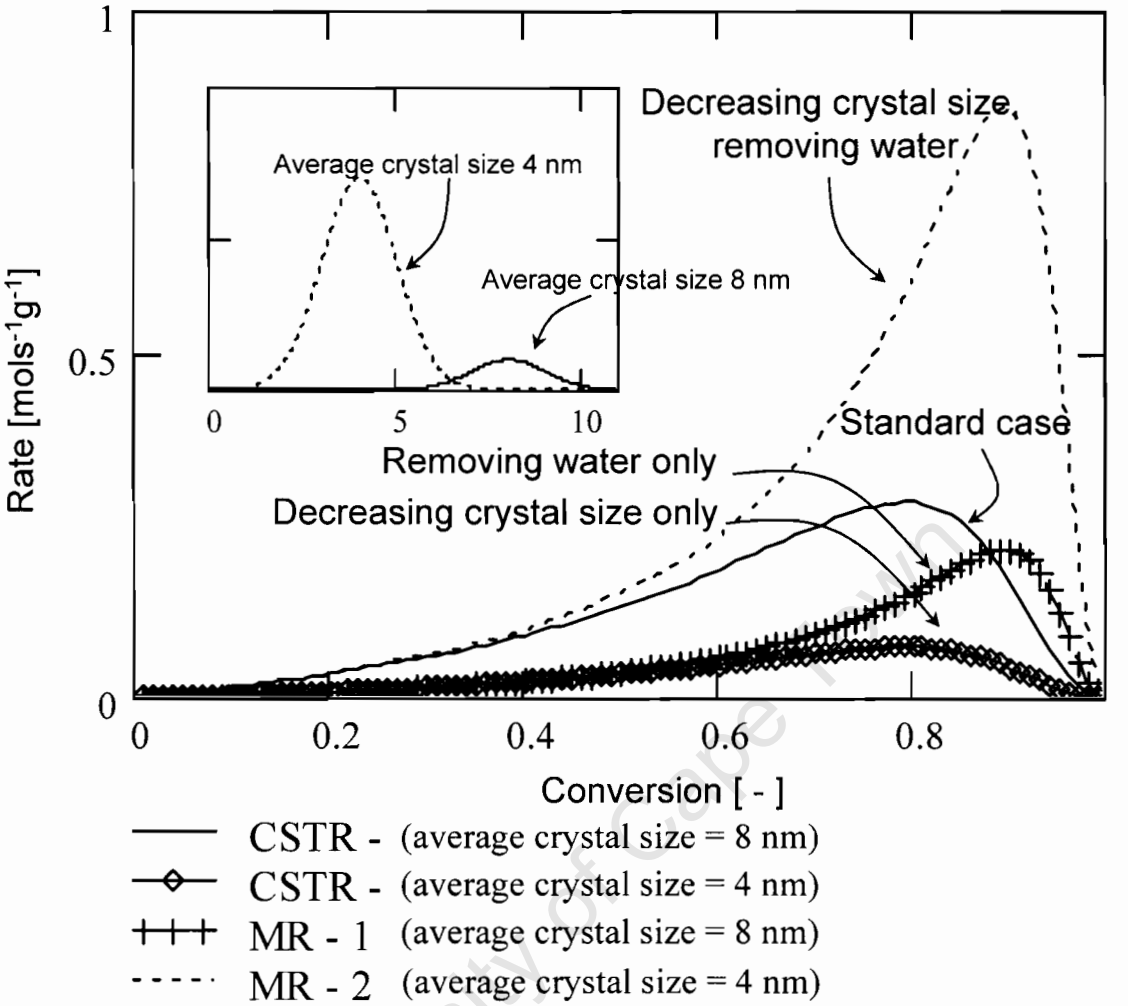

Figure 2.2: Rate of reaction as a function of conversion for different reactor configurations and crystal sizes. See text for details.

Zeolite membranes are a subset of inorganic membranes with a micro-porous structure. There has been a marked increase in the number of patents and publications on zeolite membranes within the last two decades (Caro *et al.*, 2000). Zeolite membranes are very interesting for many industrial applications (Caro, 2004) due to:

- the micro-porous structure, with pores ranging from 3-15 Å, similar to the kinetic diameter of many important industrial chemicals,
- the negative framework charge,
- their ability to withstand harsh thermal and chemical conditions of most industrial processes.

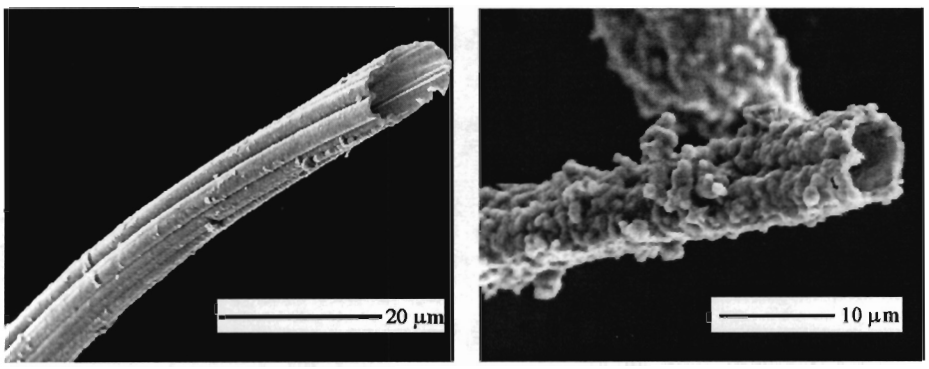

Figure 2.3: Zeolite films grown in carbon nano-tubes.

Possible industrial applications of zeolite membranes include:

- catalysis,
- membranes,
- membrane reactors,
- electronic functions, and
- optical sensors.

Before looking at any other aspects of membrane separations, it is useful to take note of kinetic diameters of species of interest as well as the structure and pore size of the zeolite membrane in question (discussed in detail in following sections). This is critical since species that cannot fit into the pores of the zeolite cannot permeate through these channels. They can only permeate through defects (Hedlund *et al.*, 1999). Table 2.1 gives calculated Lenard-Jones kinetic diameters of selected molecules of interest in the FTS as well as others used in characterisation of membranes.

2.2.1 Synthesis

There are two basic techniques for membrane synthesis. One approach uses hydrothermal synthesis where as the other uses vapour transport methods. Both techniques can be further subdivided based on the use of seed crystals. This section will give a description of the different techniques for synthesis.

Hydrothermal synthesis, also referred to as direct synthesis, is the more frequently used method. The support is treated with an appropriate solution under

Table 2.1: Lenard-Jones kinetic diameters of some species of interest

Species	Kinetic diameter (Å)
Water	2.6
Helium	2.6
Hydrogen	2.9
Nitrogen	3.6
Carbon monoxide	3.8
Methane	3.8
Methanol	3.8
n-hexane	5.0
Sulphur hexafluoride	5.5

hydrothermal conditions. The mechanism of growth is not yet clear. Suggested mechanisms include initial growth of micro crystals to fill voids in the support, or adsorption of gel into the support, or even combinations of these.

Zeolite films can also be made by treatment of a dry gel with steam at high temperatures. Xu *et al.* (1990) first described this method, and suggest a direct conversion and restructuring to a crystalline phase. It has also been suggested that the water acts as a liquid bath for dissolution and crystallisation (Chaing and Chao, 2001). The preparation of gel films is not easy. Defect free films can form only if the sol is very thin, which in turn means that a low viscosity sol must be produced. The low viscosity sol can then penetrate the support.

For the synthesis of thin uniform films seeding techniques may be applied. In this case the support is seeded with crystals prior to synthesis. The crystals can affect film orientation as well as alter the growth behaviour of the zeolite. This technique is used to control the crystal orientation and allows for defect free thin films (Chaing and Chao, 2001). The seeding of supports can be achieved by simply rubbing of pellets onto the support, or by using colloidal zeolite seeds using charged surfactants. Uniform seeding is crucial as this can largely affect the quality of membrane produced.

2.2.2 Membrane support

Zeolites membranes have been synthesised without support (Chaing and Chao, 2001). However, in order to reduce the resistance to flow it is desirable to have thin membranes (<2 μm). The support is required as these thin membranes do not have high mechanical stability and without the formation of composite membranes would be mechanically unstable. Supports must be highly porous materials,

commonly stainless steel or ceramics are used. In research, disks or tubular supports are most commonly used. However, for industrial application these are not desirable, rather multi-channel monoliths or hollow fibres are favoured due to their higher unit surface area (Chaing and Chao, 2001). Supports can be symmetric or asymmetric. Symmetric supports have a uniform pore size of about 100 nm, and asymmetric supports have a varying pore size of about 60-200 nm, with the wide pores away from the deposited zeolite.

The advantage of using stainless steel supports is that they can be very easily sealed at high temperatures. However, the main disadvantage is that of the large difference between thermal expansion coefficients of the zeolite and metal, which can cause defects. Ceramic alumina based supports are often used in literature. These are commercially available as ultra-filtration membranes. These have much closer thermal expansion coefficients to zeolites. Under the given synthesis conditions of high temperatures and pH, some leaching of the alumina into the synthesis solution may occur. The α-alumina form has low tendency to leach, whereas the γ-form must be protected during synthesis. Sealing of ceramic membranes is not simple especially at high temperatures. Other dense oxides may also be used such as SiO_2, TiO_2, and ZrO_2 (Caro *et al.*, 2000).

Supports are commonly masked before synthesis in order to ensure that zeolite is not deposited in the substrate structure. Such deposition would increase the mass transfer resistance to flow and may influence defect formation at high temperatures due to the different thermal coefficients (Chaing and Chao, 2001). There are several techniques available for masking, including filling of support with wax before synthesis (Hedlund, 2002), covering one side of the support with Teflon so that the film only grows on one side of membrane (Gora *et al.*, 2004), and positioning of the membrane so that only part of it is in contact with the synthesis solution (Chaing and Chao, 2001).

2.2.3 MFI zeolite membranes

Of the wide variety of zeolites synthesised to date, there is only a handful that have been synthesised successfully as films. MFI, LTA, MOR and FAU are the most frequently studied and most reproducible. The MFI group has gained much interest as many important industrial hydrocarbons have a similar kinetic diameter to the MFI pore dimensions. Figure 2.4 shows the MFI framework structure. The zigzag channels (running along the crystal a-axis) have pore dimensions of 5.5×5.1 Å and the straight channels (running along the crystal b-direction) have pore dimensions

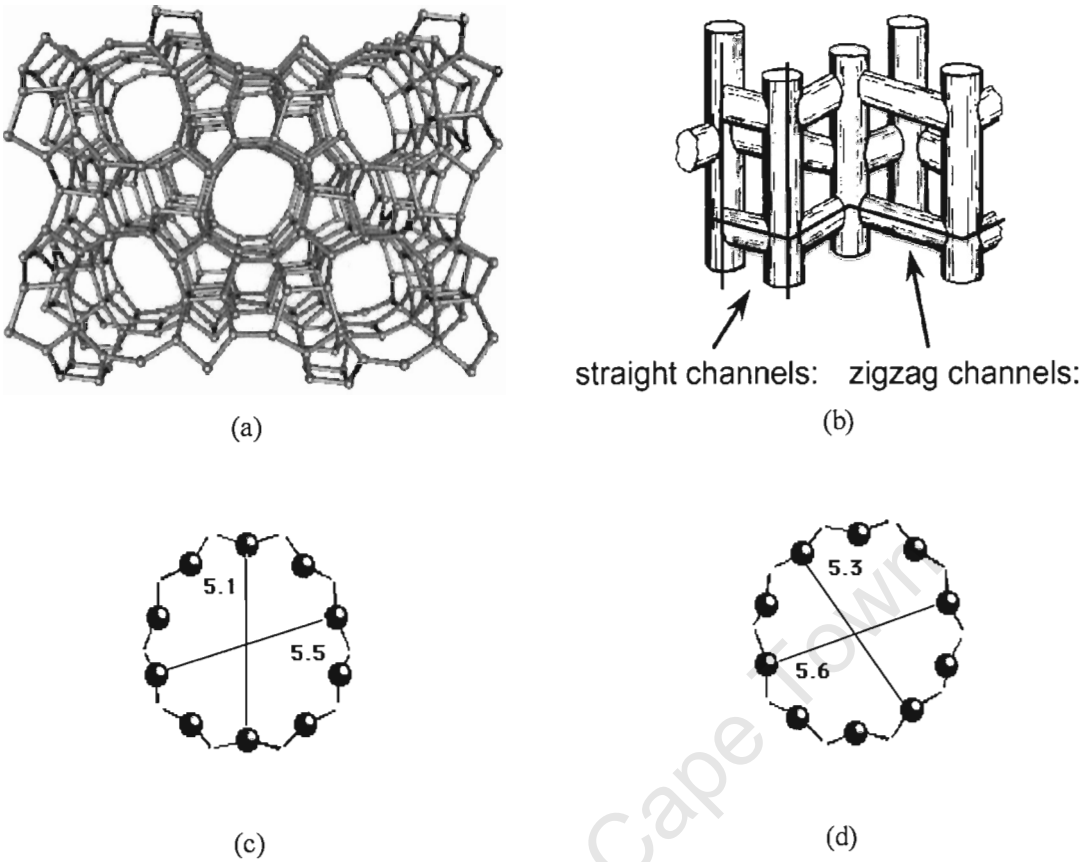

Figure 2.4: Micro-porous MFI structure (Bowen *et al.* ,2003) (a) using a stick model, (b) the channels configuration, ie. straight and zigzag channels, (c) pore dimensions (Å) along the a-axis (straight), and (d) along the b-axis (zig-zag).

of 5.6×5.3 Å. One advantage of the MFI type zeolites is that the alumina content of the zeolite can be controlled. The aluminium free form is referred to as Silicalite-1 and the analogous structure containing aluminium is called ZSM-5. Synthesis is commonly carried out under hydrothermal conditions, and with or without the aid of a structure directing agent (template) depending on the desired aluminium content. This template remains in the pores of the zeolite after synthesis and must be removed to render the micro-porous structure useful. The general formula for the MFI structure can be written as:

$$|M_n^+(H_2O)_{16}|[Al_nSi_{96-n}O_{192}] \tag{2.2}$$

with n < 27, and M^+ the metal counter-ion. However, it must be noted that it is very difficult to synthesis the ZSM-5 with Si/Al ratio <10.

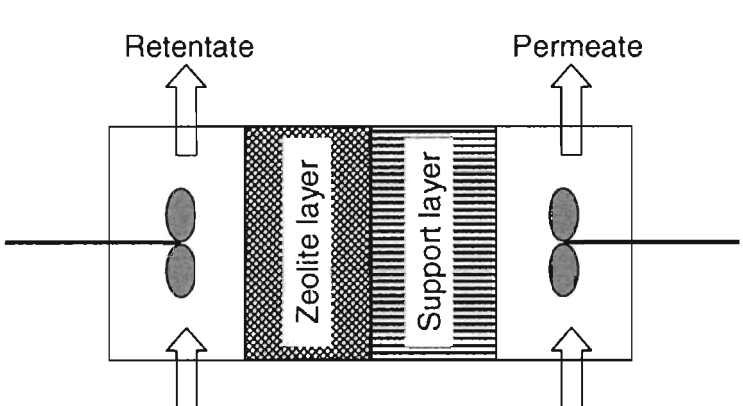

Figure 2.5: The Wicke-Kallenbach test unit, with streams in and out labelled using standard terminology.

2.2.4 Definition of permeance and selectivity

Figure 2.5 represents the Wicke-Kallenbach cell concept the most common configuration for mixture separations testing. There are usually two inlets, feed and sweep, and two outlets, retentate and permeate. The retentate is the part of the feed that does not pass through the membranes and is retained, whereas the permeate is that part of the feed that has passed through the membrane (Seader and Henley, 1998). The sweep gas is optional with the advantage that it increases the driving force across the membrane by removing the permeate as it appears. Film thickness (δ) usually refers to the thickness of the zeolite layer and excludes the support.

From a mass balance around the cell, the flux and permeance can be calculated. Flux is defined as the flowrate of a species across the membrane per unit area. Permeance is defined as the ratio of flux (J_i) and partial pressure difference (ΔP_i) of a species across the membrane as shown in equation 2.3:

$$\pi_i = \frac{J_i}{\Delta P_i} \tag{2.3}$$

The ideal selectivity (or permeance ratio or ideal seperation factor) is commonly used as a characterisation tool. The ideal selectivity is calculated from single gas permeance measurements. It is very important that these measurements are carried out at the same experimental conditions (e.g. same temperature and partial pressure difference) as results can vary if conditions are changed. Ideal selectivity

can be calculated from equation 2.4 :

$$\alpha_{i,j}^{ideal} = \frac{\pi_i}{\pi_j} \tag{2.4}$$

The separation factor (separation selectivity) is used to evaluate the mixture separation capacity of membranes. The classic definition of separation factor for membranes is similar to the definition of relative volatility in distillation (Seader and Henley, 1998), that is the ratio of compositions in the two outlet streams; equation 2.5:

$$\alpha_{i,j} = \frac{(x_i/x_j)_{permeate}}{(x_i/x_j)_{retentate}} \tag{2.5}$$

However, other definitions that are sometimes more convenient to use. Often the separation factor is not calculated using the two outlet streams. The ratio of compositions of the feed is used rather than the retentate, equation 2.6, assuming that the two streams have a similar composition. The assumption that the feed and retentate have a similar composition can be valid in cases where feed and sweep gas are well mixed, and when the flowrate of the feed and the retentate much are higher than the flux through the membrane.

$$\alpha_{i,j} = \frac{(x_i/x_j)_{permeate}}{(x_i/x_j)_{feed}} \tag{2.6}$$

In some cases the separation factor is calculated as the permeance ratio between the permeate and the feed divided by the ratio of the feed flowrates, equation 2.7. However, this definition is only correct if the partial pressure of species in the feed is the same. If a mixture is fed to the system where the partial pressures are different, large deviations from equations 2.5 and 2.6 are possible as the numerator in equation 2.7 is dependant on the partial pressure across the membrane. Hence separation factors can be very misleading.

$$\alpha'_{i,j} = \frac{(\pi_i/\pi_j)_{permeate}}{(F_i/F_j)_{feed}} \tag{2.7}$$

2.3 Characterisation of zeolite membranes

The characterisation of membranes yields important data about properties of the membrane as well as quality of the membrane. The following sections will give some detail about common techniques used for characterisation of the physical and

Table 2.2: Techniques used for physical characterisation and the information that is acquired from them

Technique	Acquired information
Scanning Electron Microscopy (SEM)	Film thickness and morphology
X-ray Diffraction (XRD)	Type, crystallinity and orientation
Atomic Force Microscopy (AFM)	Film smoothness
Inductively Coupled Plasma Spectroscopy (ICP)	Zeolite composition
N_2 adsorption	Pore volume

transport properties of zeolite membranes.

2.3.1 Membrane physical properties

The film thickness, morphology, type of zeolite, crystallinity, smoothness, zeolite composition, and pore volume of the membrane are of interest in characterisation. Common techniques for determining these are given in table 2.2.

2.3.2 Membrane transport properties

The transport properties of the membrane are used as a criteria for qualitative or quantitative characterisation of the quality and defect distribution of a given membrane. This is also essential when trying to compare membranes. Common methods of characterising membrane transport properties include:

- flux or permeance,
- ideal selectivity,
- perm-porosimetry, and
- mixture separation selectivity.

The flux or permeance through the membrane gives little information about the quality of a membrane. Ideal selectivity is more commonly used for qualitative characterisation. Different criteria have been set by different groups to characterise high quality membranes. Funke *et al.* (1996) postulate that MFI membranes can be rendered high quality if the ideal selectivity N_2 to SF_6 is greater that 80 at room temperature. The SF_6 can not travel in the zeolitic pores and so permeance of this species can only be via defects. Van de Graff *et al.* (1998) used the ideal selectivity of normal butane to iso-butane to grade the quality of their membranes. If the ideal selectivity is higher than 10 then the membrane is of a high quality.

Hedlund *et al.* (2003) suggest that high ideal selectivities may be as a result of extra diffusion resistances such as grain boundaries. Light gases such as N_2 and H_2 have high permeance through grain boundaries whereas bulkier molecules such as SF_6 have a much slower permeance resulting in an apparent high quality membrane. More recently, Deckman *et al.* (2001), Hedlund *et al.* (2003), Lai *et al.* (2003) and Clark *et al.* (2004) use perm-porosimetry to quantitatively characterise defects. Perm-porosimetry is a technique where the flux of a non-adsorbing (weak adsorbing) species is measured as a function of the relative pressure of a strongly adsorbing species. With increasing the partial pressure of the adsorbing species, pores of a certain size are blocked hence reducing the flux of the non-adsorbing species which can only travel through defects. Depending on the zeolite structure, different adsorbents are required for accurate measurements.

Finally, the mixture separation selectivity of a membrane is often investigated, as this is the most important criterion for application of membranes. However, there are many factors that can influence the separation selectivity in membranes hence this method is specific to the particular membrane. These factors will be discussed further in a separate section.

2.3.3 Defect formation

The quality of membranes produced is of utmost importance. There are three general forms of defects:

- incomplete films,
- open grain boundaries, and
- cracks.

Incompelete films are simply when a continuous film is not present, possibly due to uneven seeding or inadequate hydrothermal synthesis. Open grain boundaries occur due to a change in direction of growth of crystals. There are several mechanisms postulated to explain crack formation. Den Exter *et al.* (1997) have proposed that shrinkage of the a-direction and expansion of b-direction may cause cracks during calcination. Differences in expansion coefficients of zeolite and support may cause stress, weaken the attachment of the zeolite to the support and cause crack formation (Chaing and Chao, 2001). Large defects can be observed by SEM, but small cracks are not easily found under a microscope. Jareman *et al.*

(2004) have used n-hexane perm-porosimetry to calculate defect diameters and the width between defects for defect diameter between 1.0 to 100 nm.

2.4 Factors affecting permeance and selectivity

Several synthesis and external factors can affect the permeation and separation capacity of zeolite membranes. Temperature and species adsorption strength will be discussed in detail in other sections. The following is a list of other factors that can impact on permeance through a membrane, and its selectivity:

- type of zeolite structure synthesised,
- synthesis time and temperature,
- source and composition of synthesis solution,
- orientation of the crystal structure,
- type of support used,
- pre and post synthesis treatment, and
- presence of a sweep gas and its' flowrate.

Depending on the zeolite structure, pore geometry and size can vary. Different zeolite membranes would have different molecular sieving effects. The synthesis time and temperature define the crystalinity and more importantly the film thickness. With increasing film thickness, the mass transfer resistance increases, therefore a lower permeance is observed through the membrane. The type of support used can increase the mass transfer resistance. The interaction of the support with the zeolite can also affect zeolite growth (Gora *et al.*, 2004) hence improving the quality.

The source and composition of the membrane defines the Si/Al ratio. This is of special importance as the hydrophilicity or hydrophobicity of the membrane is a function of the Si/Al ratio. Piera *et al.* (1998) show that with decreasing Si/Al ratio of a zeolite the hydrophilicity will increase and hence increase adsorption of more polar species. Bowen *et al.* (2004) give the definition of hydrophobicity index as the ratio of organic adsorbed species to adsorbed water under the same conditions. The hydrophilic nature of zeolites with a high aluminium content is due to aluminium being trivalent. Therefore it requires a charge balancing cation and the localised electrostatic dipoles result in a hydrophilic structure. Further more ion

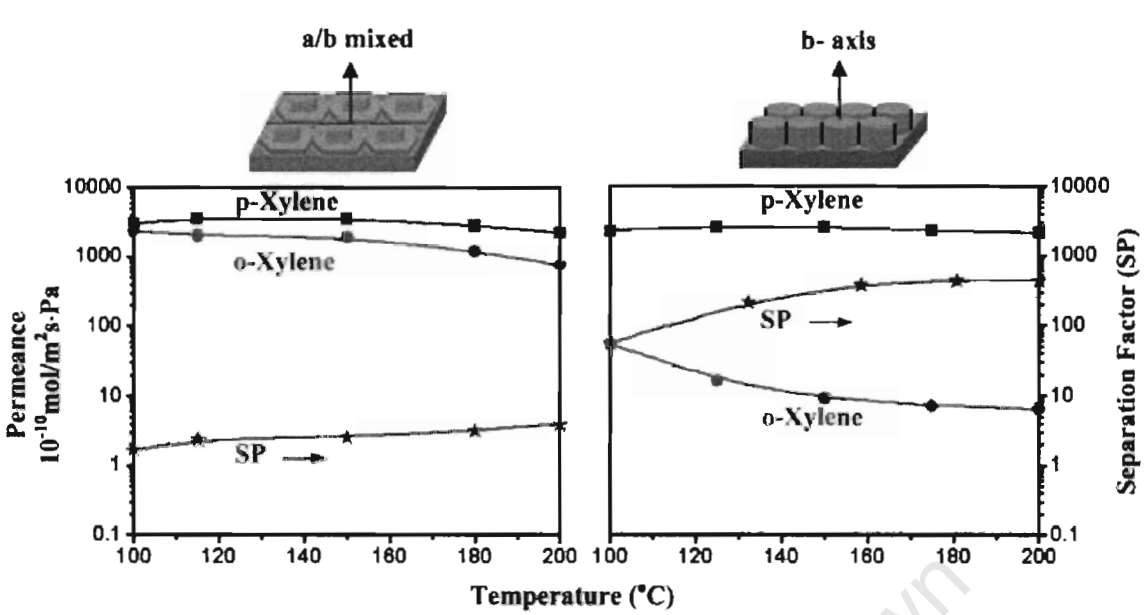

Figure 2.6: Effect of crystal orientation on the permeance and selectivity of MFI membranes, (a) with a/b-axis mixed crystal orientation, and (b) with b-axis orientation (Lai et al, 2003).

exchange and pore structure may affect hydrophilicity. Ion exchange of membranes with cations of different sizes and polarities will change the pore size and also the hydrophilic nature of the zeolite (Bowen *et al.*, 2004).

It must be noted that comparison of the hydrophilicity/ hydrophobicity nature of different zeolite structures may not give a clear indication to the actual effects as other factors such as pore geometry, size and film thickness will also affect measurements.

Recent research has clearly shown that the crystal orientation of MFI zeolite membranes can have a major effect on the permeance and separation factors for separation of xylene isomers (Lai *et al.*, 2003). These researchers used different structure directing agents to control the crystal orientation of their membranes. Figure 2.6 shows an increase in separation factors of two orders of magnitude between two membranes, one with a mixed a/b-axis and the other with b-axis orientation. The increased separation factors may be due to the b-axis oriented membranes allowing faster transport of p-xylene in the straight channels and a reduced o-xylene permeance (Lai *et al.*, 2003). Similar differences were observed for c-orientated films.

The most common pre-synthesis treatment, now becoming standard, is seeding of membranes. Using seeds ensures a higher quality film with few defects hence reducing the film thickness. It has also been suggested that using seeds may allow control over the orientation of zeolite crystals (Mintova *et al.*, 1998).

Post synthesis treatments include washing membranes to remove amorphous synthesis material. If a structure directing agent has been used, this must be removed. Removal is usually achieved by calcination: thermal oxidation of the membrane in air at high temperature. The heating and cooling rate of membranes is important. Common procedure is to calcine at up to 500°C with heating rates of 1 K/min (Piera *et al.*, 1998 and Jareman *et al.*, 2005). Jareman and co-workers investigated calcination rates and conclude that calcination at up to 5K/min does not lower the quality of the membrane produced. If no structure directing agent is used in the synthesis solution, the membranes should still be dried in order to remove adsorbed species such as water. If the membranes are not adequatly dried during permeation experiments, lower fluxes will be observed (Caro *et al.* 2000).

The presence of the sweep gas ensures that the permeate is removed as it passes through the membrane maximizing the driving force across the membrane. The only exception to this is when the permeate is valuable and dilution by increasing the sweep gas flowrate is not desired. The higher the flowrate of the sweep gas, the faster the permeate is removed hence maintaining driving force. Work done on the effect of sweep gas flowrate on permeance has shown that above a certain sweep gas flowrate there is no longer an improvement and the permeance levels off as a function of sweep gas flowrate (Salomon *et al.*, 2000 and Bernal *et al.*, 2002).

2.5 Water selective membranes

The only brief reference to the use of membranes for the FTS is Espinoza *et al.* (2000), a preliminary study for the use of zeolite membranes for water removal in FTS. Even so, there are several examples of water separations, using zeolite membranes in literature. Most of these investigate pervaporation of solvent/water mixtures using NaA membranes. Table 2.3 shows some examples of reaction/separation processes in literature, where water was selectivity removed.

Galucci *et al.* (2003) used zeolite NaA membranes for the hydrogenation of CO_2 into CH_3OH. As a result of water removal, the conversion of CO_2 and selectivity towards CH_3OH increases in comparison to traditional reactor. Zeolite A is also used for the first large scale industrial dehydration plant (Morigami *et al.*, 2001) and

Table 2.3: Previous application of zeolite membranes for separation of water

Reaction/ separation	Membrane type	Liquid/ gas phase	Reference
Knoevenagel	ZSM-5/NaX	Liquid	Lai *et al.* (2003)
Esterification	ZSM-5	Liquid	Bernal *et al.* (2002)
CO_2 hydrogenation	NaA	Gas	Gallucci *et al.* (2003)
MTBE synthesis	NaA/Mordenite	Gas	Salomon *et al.* (2000)
Pervaporation	NaA	Liquid	Morigami *et al.* (2001)
Vapour separation	ZSM-5/Mordenite	Gas	Piera *et al.* (1998)
Vapour separation	ZSM-5	Gas	Hedlund *et al.* (1999)
Vapour separation	NaA	Gas	Gora *et al.* (2004)

other solvent purifications (Urtiaga *et al.*, 2003 and Li *et al.*, 2003). However, under hydrothermal conditions and in the presence of acids these membranes are unstable. Furthermore, due to the small pore structure of LTA zeolites, the permeance of water is low compared to other membranes. This means that an unrealistic membrane surface area is required for application in FTS. Bernal *et al.* (2002) used ZSM-5 membranes to integrate reaction and separation of ethanol esterification with acetic acid. The removal of water increases conversion and selectivity. Lai *et al.* (2003) have used hydrophilic ZSM-5 membranes in the liquid phase Knoevenagel condensation reactions to remove water. By doing so they can reduce catalyst poisoning and shift the equilibrium conversion by removing a product. Piera *et al.* (1998) also use ZSM-5 and Mordenite membranes for separation of water/organic vapour mixtures.

A direct comparison between work done by these researchers is not possible as different type membranes are used for different reactions at different temperatures. For a comparison Gora *et al.* (2004) use NaA membranes which are 3 μm thick carry out binary H_2O/H_2 mixture separations. They report H_2 permeance of 2.5 $\times 10^{-8}$ mol.m^{-2}.s^{-1}.Pa^{-1}, and H_2O permeance of 2×10^{-6} mol.m^{-2}.s^{-1}.Pa^{-1}. The binary separation selectivity is 80. Hedlund *et al.* (1999) use hydrophilic ZSM-5 (Si/Al$\approx$10) membranes which are 1.8 μm thick and carry out pure component water and hydrogen measurements on wet membranes. They report selectivities of 22, significantly less than Gora *et al.*, however these membranes have a much higher water flux, 6.8 $\times 10^{-5}$ mol.m^{-2}.s^{-1}.Pa^{-1}. This can be highly beneficial in large scale utilization of zeolite membranes as a high flux membrane is required to produce a membrane with a realistic surface area.

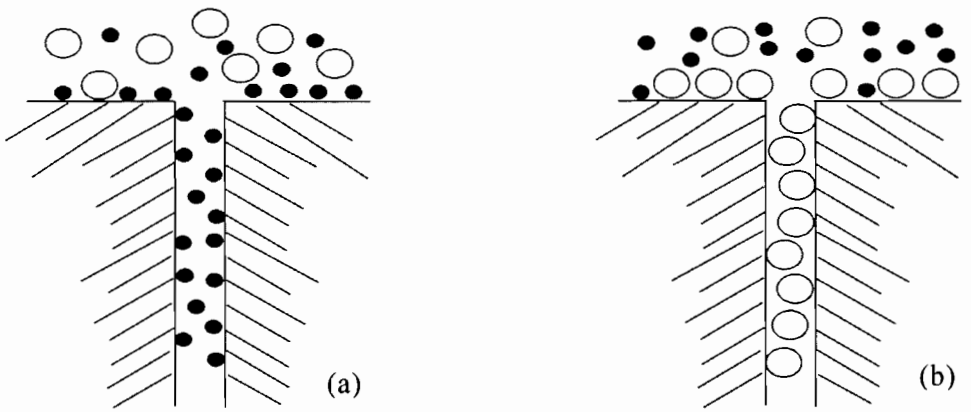

Figure 2.7: Effect of adsorption on selectivity of different species, (a) strong adsorption of small molecules, and (b) strong adsorption of large molecules.

2.6 Permeation mechanisms in zeolite membranes

The dominant mechanism for transport in defect-free zeolite membranes is micro-pore diffusion. It must be noted that the quality of the membrane can affect the dominant mechanism. If the membrane is not defect-free then knudsen diffusion and Poiseuille flow will be the dominant mechanisms as their contribution to the total permeance is much higher.

2.6.1 Micro-pore diffusion

Micro-pore diffusion is the predominant mechanism of transport in high quality zeolite membranes. Micro-pore diffusion is an activated process (Do, 1998). This means that species interact with the surface of the matrix that they diffuse in. Hence in micro-pore diffusion species must adsorb to diffuse. This leads to two possible types of micro-pore diffusion (Sommer *et al.*, 2003):

- solid vibration model, for strong adsorbing species, and
- gas translation model, for weak (negligible) adsorbing species.

Assuming that both species can get into a zeolite pore such as in figure 2.7 and that the solid vibrational model can be applied, if the small species adsorbs on the surface more strongly (figure 2.7(a)) then they block the path of the larger species. However, if the larger species adsorbs more strongly onto the surface (figure 2.7(b)) then the path of the smaller molecules is blocked. For a gas translational model, separation is based on the independent diffusion of species only. In many cases

some species in a system will permeate by solid vibrational model whereas others permeate by gas translational model, making for interesting separation dynamics (Wesselingh and Krishna, 2000).

Diffusion and adsorption of species is temperature dependant and can be described by the Arrhenius expressions:

$$K_i = K_i^o \exp\left[\frac{-\Delta H^{ads}}{RT}\right] \tag{2.8}$$

$$Đ_i = Đ_i^o \exp\left[\frac{-E_a^{sur}}{RT}\right] \tag{2.9}$$

The amount of adsorbed species on the zeolite decreases with increasing temperature, hence the heat of adsorption, ΔH^{ads} in equation 2.8, is negative. The activation energy for surface diffusion, E_a^{sur} in equation 2.9, is the energy a molecule must overcome to move from one site to another, and is usually between 5 and 60 KJmol^{-1}. K_i^o and $Đ_i^o$ are the adsorption and diffusivity pre-exponential factors. If one species cannot enter the pores there is a molecular sieving effect. In a high quality membrane the permeance is zero for a species that can not enter the pore.

2.6.2 Knudsen diffusion

Knudsen diffusion occurs when permeating molecules have a higher probability of collision with the wall than with themselves. The knudsen number, the ratio of the mean free path of a given species and pore diameter, is used as a reference point for estimating when knudsen diffusion may occur (Do, 1998). Knudsen diffusion can be calculated from equation 2.10 below:

$$Đ_{K,i} = \frac{4}{3} K_0 \sqrt{\frac{8RT}{\pi M_i}} \tag{2.10}$$

Knudsen diffusion is undesired in zeolite membranes. This type of diffusion occurs within the defects of a membrane and essentially results in lowered selectivity. Depending on the permeating species, knudsen diffusion often occurs in pores of diameter 10-100 nm. As these fall within the meso-porous regime it means that species will not be permeating via the zeolitic micropores, hence an increase in the permeance but a lowered selectivity. Ideal selectivity for knudsen diffusion given by the square root of the ratio molecular weights of permeating species as in equation

2.11:

$$\alpha_{i,j}^{k,ideal} = \sqrt{\frac{M_j}{M_i}} \tag{2.11}$$

2.6.3 Viscous diffusion

Viscous flow occurs when a pressure gradient is applied over large pores of capillaries. This flow regime is highly undesirable in membranes as essentially no separation takes place during viscous flow. The viscous diffusion coefficient can be written as:

$$Đ_{v,i} = \frac{B_0 p_i}{\nu_i} \tag{2.12}$$

2.7 Modelling of separation in zeolite membranes

With an increasing interest in membranes and permeation experiments, there is a need to theoretically explain and understand observed results. Modelling single species diffusion in membranes is relatively simple compared to binary and multicomponent diffusion. This is mainly as a result of competitive adsorption and diffusion which has a significant effect on permeation of species.

Modelling can fall into two categories: micro and macro scale modelling. Micro modelling is based on atomic scale and takes into account quantum mechanics. Although these models tend to be accurate they are highly time consuming. Common techniques include: force field, Monte-Carlo simulations and molecular dynamics (Kärger and Ruthven, 1992). These have the advantage of using techniques that provide an easy way to investigate effects such as channel geometry and structural heterogenity, but long computation times are required (Kärger and Ruthven, 1992). Macro scale modelling on the other hand is much faster. The most common applied method for modelling mixture permeance is the Maxwell-Stefan approach. More simplified models such as activated diffusion, and Fick's law (Do, 1998) can also be applied. It must be noted that models ignore support effects and assume that the membrane is defect free, which is never true. These assumptions may lead to large deviations.

2.7.1 Maxwell-Stefan approach

The generalised Maxwell-Stefan (MS) equations are derived from a force balance between molecules. To effect a relative motion between species, a driving force must be applied, the chemical potential gradient. This driving force is balanced

by a frictional force between diffusing species. The generalised Maxwell-Stefan equation, equation 2.13, is derived from the theory of irreversible thermodynamics (Taylor and Krishna 1993):

$$\frac{x_i}{RT}\nabla\mu_i = \sum_{\substack{i=1 \\ j\neq i}}^{n} \frac{x_j N_i - x_i N_j}{C_t Đ_{ij}} \tag{2.13}$$

In the application of Maxwell-Stefan equations to multi-component surface diffusion in zeolites, the zeolite matrix is the $(n+1)^{th}$ component (Krishna, 1990) with a fractional occupation proportional to the molar fraction (Wesselingh and Krishna, 2000). However, as the zeolite is not in motion it is essentially stagnant. Equation 2.14 represents the modified MS equation for diffusion in zeolites (Krishna and Baur, 2003). θ_i (surface composition of species) in equation 2.14 is the equivalent to x_i (mole compossion of species) in equation 2.13. The model can hence be applied to multi-component mixtures where competitive adsorption and diffusion play roles in the rate of diffusion (Kapteijn *et al.*, 1995).

$$-\rho\frac{\theta_i}{RT}\nabla\mu_i = \sum_{\substack{i=1 \\ j\neq i}}^{n} \frac{\Theta_j N_i - \Theta_i N_j}{\Theta_{i,sat}\Theta_{j,sat}Đ_{ij}} + \frac{N_i}{\Theta_{i,sat}Đ_i} \tag{2.14}$$

The chemical potential $\nabla\mu_i$ in equation 2.14 must be evaluated for the species in the zeolite matrix. Assuming equilibrium between the sorbed species and the bulk fluid phase (Krishna and Baur, 2003), the chemical potential can be related to the surface coverage gradient by a thermodynamic correction factor:

$$\frac{\theta_i}{RT}\nabla\mu_i = \sum_{j=1}^{n}\Gamma_{ij}\nabla\theta_i \tag{2.15}$$

The thermodynamic correction factor, equation 2.16, relates the amount of adsorbed species to the fugacity of that species. For low system pressures the component fugacity can be approximated by partial pressure. The correction factor is as follows:

$$\Gamma_{ij} = \delta_{ij} + x_i\frac{\partial \ln f_i}{\partial x_j} \tag{2.16}$$

2.7.2 Adsorption isotherms

The Langmuir isotherm, equation 2.17, is the simplest theoretical model to describe non linear adsorption on a homogeneous surface (Krishna and Baur, 2003):

$$\theta_i = \frac{b_i p_i}{1 + b_i p_i} \tag{2.17}$$

with θ_i, the surface coverage, based on the ratio of loading and saturation loading of a species, equation 2.18:

$$\theta_i = \frac{q_i}{q_{i,sat}} \tag{2.18}$$

For multi-component systems, the Langmuir isotherm can be extended. The multi-component Langmuir isotherm is given by equation 2.19:

$$\theta_i = \frac{b_i p_i}{1 + \sum_{i=1} b_i p_i} \tag{2.19}$$

The main shortcoming of the above multi-component isotherm is that does not account of varying saturation loadings of different species. More complex isotherms can be used that take saturation loading into account. Furthermore, a dual-site multi-component isotherm is required for adsorption of branched species. This would take into account the different saturation capacities for each component in the zeolite. However, in these cases often ideal adsorption solution (IAS) and real adsorption solution (RAS) theories and simple Langmuir isotherms are currently used (Krishna and Baur, 2003).

Chapter 3

Hypothesis

3.1 Summary of literature

In the first part of the literature review, the FTS rate of reaction is shown. The effect of decreasing water partial pressure and crystal size simultaneously are described. It was shown that by reducing crystal size to less than 6 nm the cobalt catalyst for FTS deactivates. Water causes this deactivation hence motivating the incorporation of zeolite membranes to remove water in-situ.

Zeolite membranes may be used for the in-situ removal of water from the FTS due to their high thermal and chemical stability. Zeolite membranes are often supported so as to improve mechanical strength. Membranes can be synthesised by hydrothermal synthesis or vapour transport methods. The direct hydrothemal synthesis method is the most common technique. Supports are often seeded prior to synthesis to aid growth. Characterisation of physical and transport properties of membranes is essential in any study. Some of the most common techniques include SEM for film thickness, ICP for zeolite composition, and XRD for zeolite type, crystallinity, and crystal orientation. Perm-porosimetry is used for quantitative defect characterisation. Permeation experiments are conducted in a Wicke-Kallenbach cell. Flux, permeance, ideal selectivity and separation selectivity are used to describe membrane transport properties.

Factors influencing permeance and separation selectivity include film thickness, Si/Al ratio, crystal orientation, type of support used and sweep gas flowrate. Hydrophilic membranes with low Si/Al ratios are best suited for water removal. Membranes with different film thickness and zeolite stucture are used for comparison of hydrophilicity. Changes in selectivity and permeance may be due to these factors and not only due to reducing Si/Al ratio. To investigate the effect of Si/Al ratio

on hydrophilicity of membranes, this should be the only parameter changed. Water separation, using zeolite membranes in literature, were also described. Zeolite A, Zeolite X, Mordenite and ZSM-5 are most commonly used. Direct comparison of these is very difficult as parameters other than Si/Al ratio have also changed.

Mechanisms of transport in zeolite membranes include adsorption-surface diffusion in the zeolite film. The main transport mechanisms in the support and defects are knudsen diffusion and viscous flow. Maxwell-Stefan equations have been applied to model multi-component permeation in zeolite films. Langmuir isotherms are applied to describe adsorption in the MS equations.

3.2 Hypotheses

- MFI zeolite membranes can be used for selective water removal from a H_2O/H_2 mixture,
- Decreasing the Si/Al ratio of MFI zeolite will increase the H_2O/H_2 selectivity,
- Hydrocarbons reduce the water and hydrogen flux by competetive adsorption, and
- The Maxwell-Stefan model can adequately describe experimental data.

3.3 Key questions

- What is the effect of Si/Al ratio on the permeance and selectivity?
- What is the effect of temperature on permeance and selectivity?
- Can a simplified model be derived to describe the behaviour of the system?

Part II

Experimental and Model development

Chapter 4

Experimental

The following chapter outlines the experimental procedure, including support preparation, membrane synthesis, characterisation and testing.

4.1 Support masking

Commercial asymmetric α-alumina microfiltration filters (Inocermic GmbH) are used as supports for the zeolite membranes. The supports have an average pore size of 100 nm and 3 μm in the top and bottom layers respectively. The top layer and bottom layers are 30 μm and 3 mm thick respectively. The disks have a diameter of 25 mm. The supports have to be prepared for synthesis of the zeolite layer.

The masking technique was developed by Hedlund *et al.* (2002) in order to reduce the growth of zeolite into the support. By reducing support invasion, defect formation may be reduced during heating or cooling. Also deposition of synthesis materials into the support is reduced hence reducing mass transfer resistance. The membrane is filled with a material which is stable under synthesis conditions, in this case this is polyethylene wax (Exxon Chemicals, T_B=120°C). Initially the side on which zeolite is to be grown is coated with a protecting layer of polymethylmetacrylate (PMMA, Polykemi) solution, dissolved in acetone (1:3.75 by weight) as shown in figure 4.1(b). Once the polymer has dried, the support is heated at 1°C/h to 150°C in a vacuum oven. At 150°C the support is submersed upside down in molten wax and the oven is evacuated to aid complete filling of the support with wax, figure 4.1(c) and cooled again after one hour. The PMMA layer is then dissolved in acetone for one week, figure 4.1(d), to expose the surface for zeolite growth. The wax does not dissolve in acetone and only melts above the synthesis

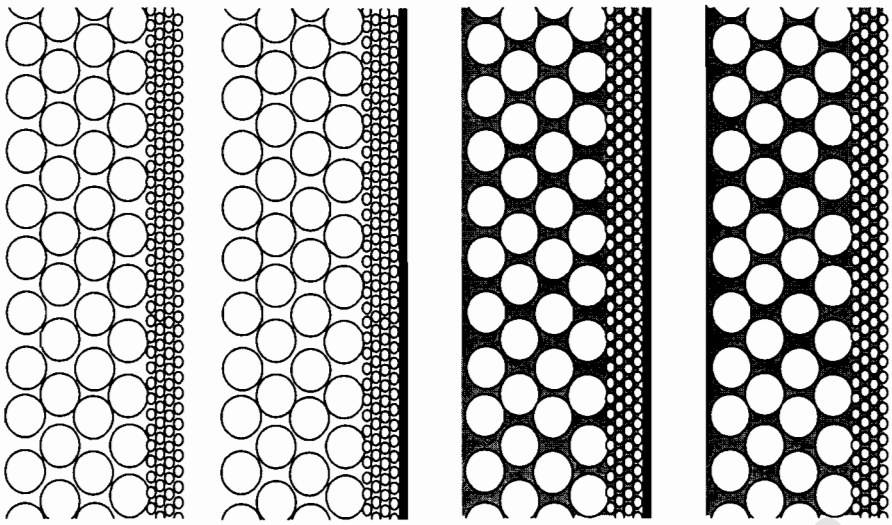

Figure 4.1: Representing the stages in masking: dry support (a), application of PMMA solution to the top surface of support (b), filling of support with wax (c), and removal of PMMA to re-expose surface for synthesis (d).

temperature hence effectively blocking zeolite growth into the support.

Masked membranes are used when the synthesis temperature is 100°C. However, for the template free membranes a synthesis temperature of 180°C is required and supports cannot be masked as the wax would melt during synthesis.

4.2 Membrane synthesis

Membranes are synthesised with and without the use of a template. Silicalite-1 and ZSM-5 (Si/Al=50) using template and ZSM-5 (Si/Al=10) are synthesised by a template free procedure. Multiple sets of membranes are synthesised in order to check reproducibility of the results.

4.2.1 Seeding

Prior to synthesis, all supports are seeded with nano-crystals in order to aid zeolite growth. TPA-silicalite-1 seeds are synthesised from a synthesis solution with composition: 9 TPAOH: 25 SiO_2: 360 H_2O: 100 EtOH. The synthesis solution is hydrothermally treated at 50°C for two months. The resulting crystals, 60 nm in

Table 4.1: Chemicals used for membrane synthesis

Chemical	Source/concentration
TPAOH	Sigma, 1.0 M
TEOS	Merck, >98%
Al-isopropoxide	Merck
$Na_2SiO_3.9H_2O$	Sigma, >98%
$Al_2(SO_4)_3.18H_2O$	Riedel-deHaen
Bindzil 30/220	Eka Nobel AB
Cationic polymer	Redifloc, 0.4 % wt
Ethanol	Merck, >99%

diameter, are purified by centrifugation at 20 000 rpm. The seeding procedure is as follows:

- wash four times with ethanol through 0.1 μm filter,
- wash four times with 0.1 M ammonia through 0.1 μm filter,
- apply cationic polymer solution with 1 μm filter and leave for 10-15 mins,
- wash four times with 0.1 M ammonia through 0.1 μm filter,
- apply seed solution with 0.2 μm filter and leave for 10-15 mins, and
- wash four times with 0.1 M ammonia through 0.1 μm filter.

The seeding of the supports is carried out in a laminar flow bench in order to minimize foreign particulates (such as dust) on the support. All solutions administered are passed through filters for the same reason. The initial washing stages are also carried out to ensure that there is no dust or other material present on the support before seeding. The cationic polymer adsorbs onto the support surface rendering it positively charged. This treatment is necessary for the adsorption of the negatively charged seed crystals. The support is rinsed in ammonia to remove excess cationic polymer. The seed crystals are then added.

4.2.2 Template assisted synthesis

For this synthesis, masked and seeded supports where immediately immersed into synthesis solutions with a molar composition 3 TPAOH: 25 SiO_2: 1450 H_2O: 100 EtOH (silicalite-1) and 3 TPAOH: 0.25 Al_2O_3: Na_2O: 25 SiO_2: 1600 H_2O: 100 EtOH (ZSM-5). Tetrapropylammoniumhydroxide (TPAOH) is the template used, the silica source is tetraethylortosilicate (TEOS), and the aluminium source is aluminium

isopropoxide (see table 4.1 for details). The synthesis solution Si/Al ratio is ∞ and 50 for silicalite-1 and ZSM-5 membranes. The synthesis solution is prepared before-hand and left to hydrolyse on a turning table overnight. The supports are placed at an angle in a holding unit facing down to avoid sedimentation and gas accumulation on the film surface. The synthesis solution is kept at 100°C (atmospheric pressure, reflux) by means of an oil bath. It is desired to have near identical film thickness for the two different films. In order to compensate for the different growth rates of silicalite-1 and ZSM-5 films, the membranes are hydrothermally treated for 36 hours and 27 hours respectively.

4.2.3 Template free synthesis

Template free membranes were synthesised using sodium methasilicate ($Na_2SiO_3.9H_2O$) aluminum sulphate ($Al_2(SO_4)_3.18H_2O$) and Bindzil 30/220 (see table 4.1 for details). The synthesis solution is prepared before-hand. $Na_2SiO_3.9H_2O$ and $Al_2(SO_4)_3.18H_2O$ are dissolved in water in separate beakers. Before synthesis the dilute silica sol is added, hence the molar composition of the synthesis solution is: 30 Na_2O: Al_2O_3: 100 SiO_2: 4000 H_2O. The synthesis solution Si/Al ratio is 50 for the template free ZSM-5 membranes. Supports are placed upside down in cylindrical teflon holders and placed into steel autoclaves. The synthesis time is 12 hours at 180°C. Due to the high temperature synthesis, supports could not be masked hence the back side of the membrane is protected using a teflon disk.

4.2.4 Post synthesis procedure

At the end of the synthesis, the membranes are removed from the synthesis solution and placed in 0.1 M ammonia for 24 hours. The ammonia is changed at least 6 times. The ammonia rinse is required in order to remove loosely attached crystals from the surface of film and any remaining synthesis solution. The template assisted membranes are calcined at 500°C for 6 hours in order to remove the template and wax. A heating rate of 0.2°C/min and cooling rate of 0.3°C/min was used in order to minimise defect formation. The membranes are kept at 110°C in order to stop adsorption of foreign species onto the films. To avoid calcination of the template free membranes, the seeded supports were calcined at 500°C for 4 hours in order to remove template from the seeds. After synthesis, these membranes were dried in-situ at 110°C for 50 hours in order to remove adsorbed species.

4.3 Membrane characterization

Membranes are characterised by SEM, XRD and n-hexane porosimetry.

4.3.1 Film thickness and Morphology

A Philips XL30 scanning electron microscope equipped with a LaB_6 emission source, running at 30 KV, is used to record SEM images in order to study film thickness and morphology of the membranes. Samples are mounted on a stub using carbon glue, and dried in an oven overnight. They are gold coated using spurting prior to image capture. Gold coating of samples is required in order to capture high magnification images. In order to determine the film thickness, the membranes have to be cracked carefully to expose the cross-section.

4.3.2 Crystallinity and zeolite type

X-ray diffraction (XRD) patterns are measured using a Siemens D5000 diffractometer. X-ray intensity is recorded as a function of the beam deflection angle (2θ). The scan range is 5 $<2\theta°<45$ at 0.02° intervals. According to Braggs law, high x-ray intensities will occur at deflection angles specific to a certain structure. In this way, the XRD pattern of an unknown sample can be compared to those already know. In the case of comparison of zeolite powers containing randomly orientated crystals with zeolite membranes, relative peak intensities will vary significantly as the zeolite membranes have orientated crystals.

4.3.3 n-hexane porosimetry

n-hexane porosimetry is used as a tool to measure the quality of the membranes synthesised. Figure 4.2 shows a schematic of the porosimetry unit where measurements were carried out. The permeance of helium is measured as a function of the relative partial pressure of n-hexane at room temperature. With an increase in the relative partial pressure of strongly adsorbing n-hexane, pores up to a certain diameter are blocked. This blockage can be measured by the decrease in helium permeance. Prior to measurements, membranes are heated to 300°C for 8 hours in a flow of dry helium in order to remove all adsorbed species. Helium is fed by means of two mass flow controllers, one directly to the cell and the other via two n-hexane saturators. This way the relative pressure of n-hexane can be adjusted over a wider range of relative pressures. One saturator is at room temperature and the other is

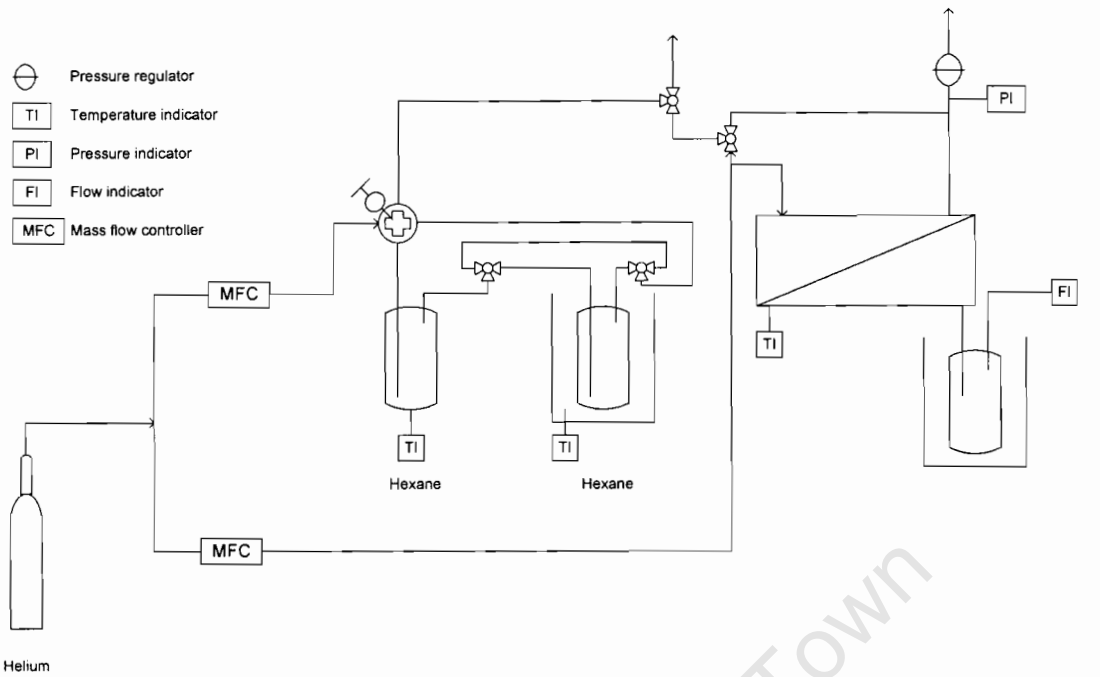

Figure 4.2: Schematic of the perm-porosimetry unit.

placed in a cooling bath. The pressure difference across the membrane is adjusted by a pressure regulator while the permeate is at atmospheric pressure, therefore the driving force for permeance is a pressure difference. The permeate passes through a cooling trap to remove n-hexane and the flowrate of helium is measured by a soap flow meter.

4.4 Permeance measurements

4.4.1 Single gas

Single gas measurements are carried out directly after calcination. The membranes were sealed with graphite gaskets in a modified Wicke-Kallenbach cell. This is achieved by sealing the sweep gas inlet and outlets. Dry nitrogen is fed to the cell during mounting. The driving force for permeance is a trans-membrane pressure difference. The feed pressure is varied from 1 to 5 bar absolute while the permeate side is at atmospheric pressure and the temperature was varied from 25°C to 300°C. The volumetric flow of pure gases is measured using a soap flowmeter at low flowrates (0-100 ml/min). At higher flowrates an electronic flowmeter (ADM 1000, J & W Scientific) is used that could measure flowrate up to 1100 ml/min. The flux

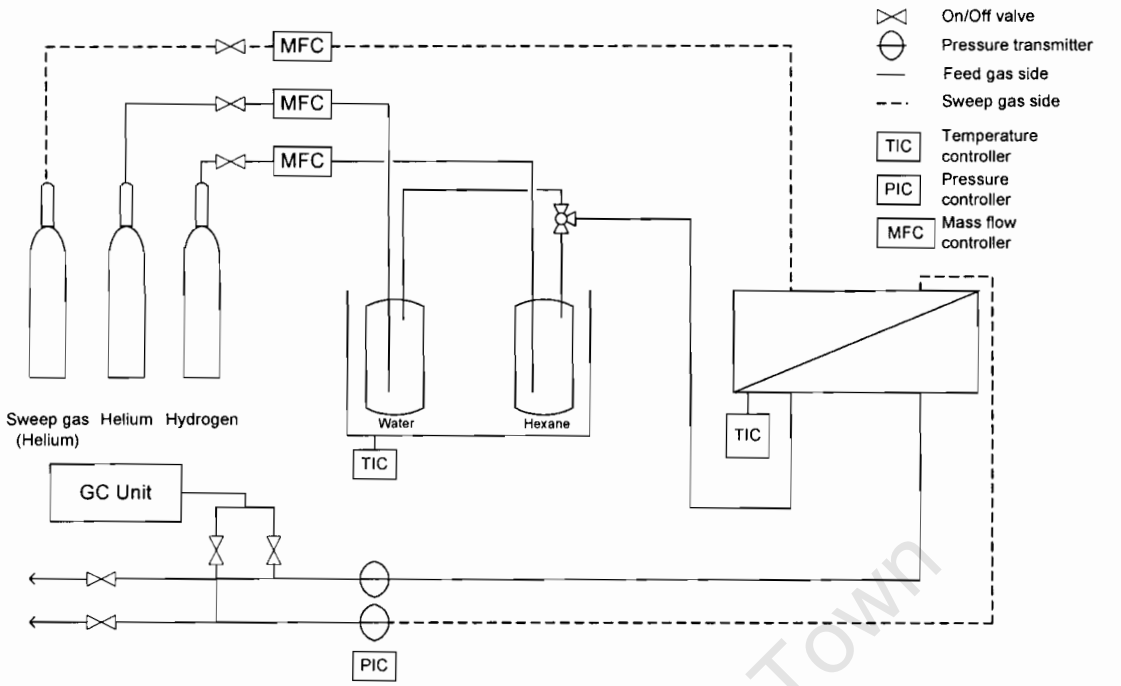

Figure 4.3: Schematic of the permeation unit.

and permeance are calculated from the volumetric flowrates using equations D.1 and D.2 from Appendix D.

4.4.2 Gas mixtures

Gas mixture permeation measurements were performed in a Wicke-Kallenbach cell (figure 2.5). Figure 4.3 shows a schematic of the permeation unit. The membranes are mounted in a stainless steel cell, sealed with graphite gaskets. For multi-component separations, H_2 and He streams are controlled by mass flow controllers. Water and n-hexane are introduced by saturators immersed in a water bath at 20°C. H_2 passed via the n-hexane bubbler and water via the water bubbler. Helium is used as sweep gas and the total pressure difference across the membrane is zero. The back diffusion of He was reduced considerably as it was the major component on both sides of the membranes, table 4.2. Hence He is assumed to behave only as a solvent. Table 4.2 shows the feed flowrates at standard pressure and temperature (STP) and compositions of the binary and ternary mixtures used in carrying out the mixture separations. The driving force for permeance is a concentration gradient in contrast to n-hexane porosimetry and single gas measurements, where the driving force is a result of a pressure difference. The pressure on both the feed and sweep

Table 4.2: Flowrates and composition of the binary and ternary mixtures

Species	Binary		Ternary	
	Flowrate (ml/min)	mol %	Flowrate (ml/min)	mol %
H_2	25	0.20	25	0.19
H_2O	2.4	0.02	2.4	0.02
n-C_6	-	-	4.8	0.04
He	100	0.78	100	0.76
Sweep gas	100	-	100	-

side is controlled using pressure controllers both set to 1 bar (gauge).

The temperature at the membrane is recorded by a thermocouple (type K) connected to the membrane cell. The cell is mounted inside an isolated furnace. During runs the furnace is programmed so that the temperature increases at 0.2-0.3°C/min. This ensures that the membrane is not damaged during heating/cooling and that the system is at pseudo-steady state. An online Varian 3800 GC equipped with a capillary column and two packed columns (molecular sieve and chromosorb) is used to separate mixtures. Samples are taken every 30-40 minutes depending on the number of samples desired. A thermal conductivity detector is used for quantitative analysis of samples. The membrane is heated to 400°C for 8 hours in a flow of dry helium prior to measurements to ensure desorption of all species.

The GC is calibrated for H_2, H_2O and nC_6 beforehand (Appendix C). The peak area is measured as a function of known species' partial pressure. The partial pressure is plotted as a function of peak area in order to calculate permeance of each species across the membrane. Species partial pressure is calculated from equation D.4 and hence flux and permeance calculated. Selectivity is calculated from equation D.3, Appendix D.

Chapter 5

Model development

Single gas permeance and mixture separations are modelled in order to understand mechanisms of transport in the membrane. In the model development certain simplifying assumption are made. The following sections will give step by step details of how models were developed and implemented.

5.1 Single component permeance

Single gas flux through the support and zeolite membrane was modelled using equation 5.1 (Do, 1998):

$$J_i = \frac{Đ_{eff,i}}{RT}\frac{dP}{dz} \tag{5.1}$$

A combined effective diffusion coefficent was used. This diffusion coefficent took into account knudsen diffusivity, equation 2.10, and viscous diffusivity, equation 2.12. The total flux is given by equation 5.2:

$$J_i = \left(\frac{8\sqrt{2}K_0}{3\sqrt{\pi M_i RT}} + \frac{B_o\overline{P}}{\nu_i RT}\right)\frac{\Delta P}{\Delta z} \tag{5.2}$$

To investigate the effect of transmembrane pressure drop, the flux J_i was plotted versus the average pressure across the membrane, $\overline{P}$, for pure component species, (e.g. figure 6.9). To investigate temperature effects, at constant ΔP, on the support equation 5.2 was linearized yielding equation 5.3.

$$J_i\sqrt{T} = \left(\frac{8\sqrt{2}K_0}{3\sqrt{\pi M_i R}} + \frac{B_o\overline{P}}{\nu_{i,0} RT}\right)\frac{\Delta P}{\Delta z} \tag{5.3}$$

Equation 5.3 takes into account the effect of temperature on viscosity, ν_i is replaced with $\nu_{i,0}$ the viscosity at a reference temperature. The effect of temperature on viscosity of pure gases calculated from the hard sphere model, equation 5.4:

$$\nu_i = 2.669 \times 10^{-5} \frac{\sqrt{M_i T}}{\sigma^2} \tag{5.4}$$

5.2 Multi-component permeance

For multi-component diffusion a simplified Maxwell-Stefan equation was developed based on equation 2.14. If the Maxwell-Stefan interaction between species i and j is very small, i.e.: $Đ_{ij} \rightarrow \infty$, then equation 2.14 simplifys to equation 5.5. This assumption is often applied in literature as it simplifies the MS equation even if it may cause significant deviations (Krishna and Baur, 2004).

$$-\rho \frac{\theta_i}{RT} \nabla \mu_i = \frac{N_i}{\Theta_{i,sat} Đ_i} \tag{5.5}$$

Flux is assumed to occur in one dimension, across the zeolite film and thus the chemical potential gradient is given by equation 5.6:

$$\nabla \mu_i = \frac{d\mu_i}{dz} \tag{5.6}$$

The chemical potential corresponds to the Gibbs' free energy. Expressed in terms of fugacity the chemical potential is given by equation 5.7:

$$\mu_i = RT \ \ln\left(\frac{\overline{f_i}}{f_i}\right) \tag{5.7}$$

with the real mixture fugacity:

$$\overline{f_i} = x_i \gamma_i f_i \tag{5.8}$$

The composition of species in the zeolite, θ_i, is equivalent to x_i and is calculated from the surface coverage of each species, based on the Langmuir isotherm, equation 2.19. Equation 5.7 then simplifies to:

$$\mu_i = RT \ln(x_i \gamma_i) \tag{5.9}$$

and the chemical potential gradient given by:

$$\frac{d\mu_i}{dz} = RT \frac{d \ln(x_i \gamma_i)}{dz} \tag{5.10}$$

Hence the flux of each species can be calculated from the simplified Maxwell-Stefan equation.

$$N_i = -Đ_i C_t x_i \frac{d\ln(\gamma_i x_i)}{dz} \tag{5.11}$$

The activity coefficent is given by equation 5.12. The activity coefficent is derived from Langmuir isotherm, equation 2.19.

$$\gamma_i = (1 - \sum x_i)^{-1} \tag{5.12}$$

The chemical potential gradient can be evaluated analytically yielding equation 5.13. It is clear that from the second part of equation 5.13 that the chemical potential of all species affect each other, hence there is a strong coupling effect.

$$\frac{d\ln(x_i\gamma_i)}{dz} = \frac{\left(1 - \sum_{j\neq i}^{n} \frac{dx_j}{dz}\right)\frac{dx_i}{dz} + x_i \sum_{j\neq i}^{n} \frac{dx_j}{dz}}{x_i\left(1 - \sum_{i=1}^{n} x_i\right)} \tag{5.13}$$

The rate of change of composition along the membrane thickness was approximated using equation 5.14. According to Wesselingh and Krishna, (2000) this approximation is very close to the actual gradient when $\Delta\overline{x}_i \ll 1$ where equation 5.14 is evaluated at the average mole fraction across the film.

$$\frac{dx_i}{dz} \approx \frac{\Delta\overline{x}_i}{\Delta z} \tag{5.14}$$

The composition of species in the zeolite were related using Langmuir isotherms, equation 2.19. The model developed accounts for flux as a function of temperature. Adsorption and diffusion are functions of temperature. The model accounts for these using equations 2.8 and 2.9.

The main shortcomings of the model are:

- The langmuir isotherm used does not account for varying saturation loadings,
- The approximation used to calculate chemical potential gradient can deviate at high surface coverage, and
- The interaction parameter may not be negligible in this system.

Part III

Thesis Results

Chapter 6

Results and discussion

The following chapter will give experimental and modelling results gathered and discuss significant features thereof.

For the synthesis of template assisted membranes outlined in the experimental section, it has been well documented that membranes have a consistently high quality (Hedlund *et al.* 2003). To ensure reproducibility of results, three replicates of each structure was fabricated and labelled Sx or Zx with S and Z denoting silicalite-1 and ZSM-5 respectively and the letter x in the label is the sample number, from 1 to 3. However, for the synthesis of the template free membranes, reproducibility was an issue as will be discussed shortly. For this reason seven replicates were synthesised in two separate batches. The as-synthesised membranes were labelled ZTFx with ZTF indicating template free ZSM-5 and the letter x in the label is the sample number, from 1 to 7.

6.1 Characterisation

SEM and XRD measurements were used to characterise membranes' physical properties. Membrane quality was characterised by single gas permeance, perm-selectivity and n-hexane porosimetry. The following sections will give details of the attained results.

6.1.1 Scanning Electron Microscopy

Figure 6.1(a) and (b) represent side and top view SEM images of the macro-porous support with an average pore size of 100 nm and 3 μm in the top and bottom layers respectively. Due to these large pores, the support would experience mostly viscous

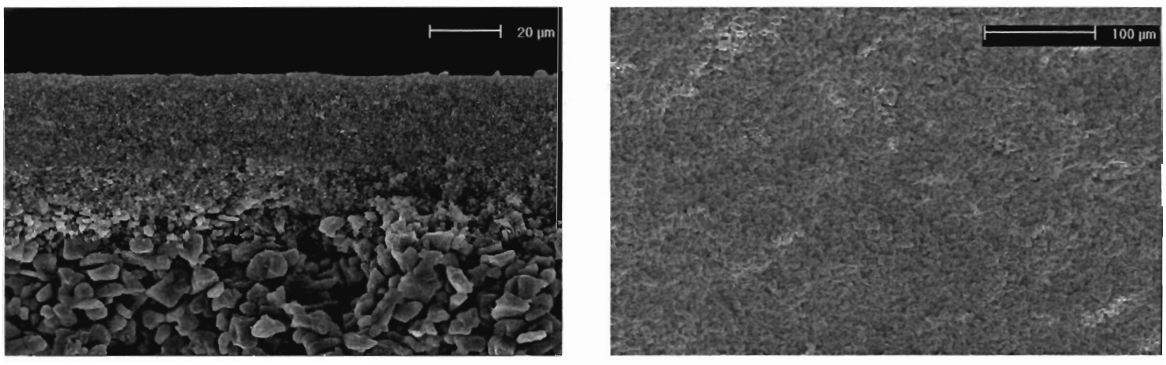

Figure 6.1: SEM images of the support (a) side and (b) top views.

flow due to the pressure gradient. It has been reported that with decreasing film thickness the resistance of the support may become the dominant effect (Chaing and Chao, 2001). At 500 nm thickness, the membranes synthesised here are much thinner than those commonly reported in literature (membranes up to 60 μm thick (Chaing and Chao, 2001) have been reported).

Zeolite membrane SEM images were recorded after all other experiments were completed, as this method is destructive. Figure 6.2(a) and (c) show side view images of S2 and Z1 membranes synthesised respectively. The film thickness was measured to be approximately 500 nm for both the silicalite-1 and ZSM-5 membranes with variations in thickness as result of the rough support surface. From figure 6.2(a) and (c) it can also be observed that no zeolite has grown into the support. This is as a result of the masking of supports.

Figure 6.2(b) and (d) show the corresponding surface images. Both films are dense and continuous. The silicalite-1 membranes showed no visible defects, however it appears that some defects were present for the ZSM-5 membranes in the form of cracks as can be observed from figure 6.2(d), indicated by the arrow. It is proposed that these defects where not present at initial testing stages and are most likely due to extensive thermal treatment of the membranes at elevated temperatures of 400°C.

Figure 6.3(a) and (b) show side and surface images of ZTF4 synthesised without the assistance of structure directing agents respectively. The film thickness of this membrane is approximately 1600 nm. There is also some zeolite growth into the support as supports were not masked before hydrothermal synthesis. Figure 6.3(b) shows a surface image of the membrane. Continuous, well-defined crystals have formed in the template free membranes which were not present in the template as-

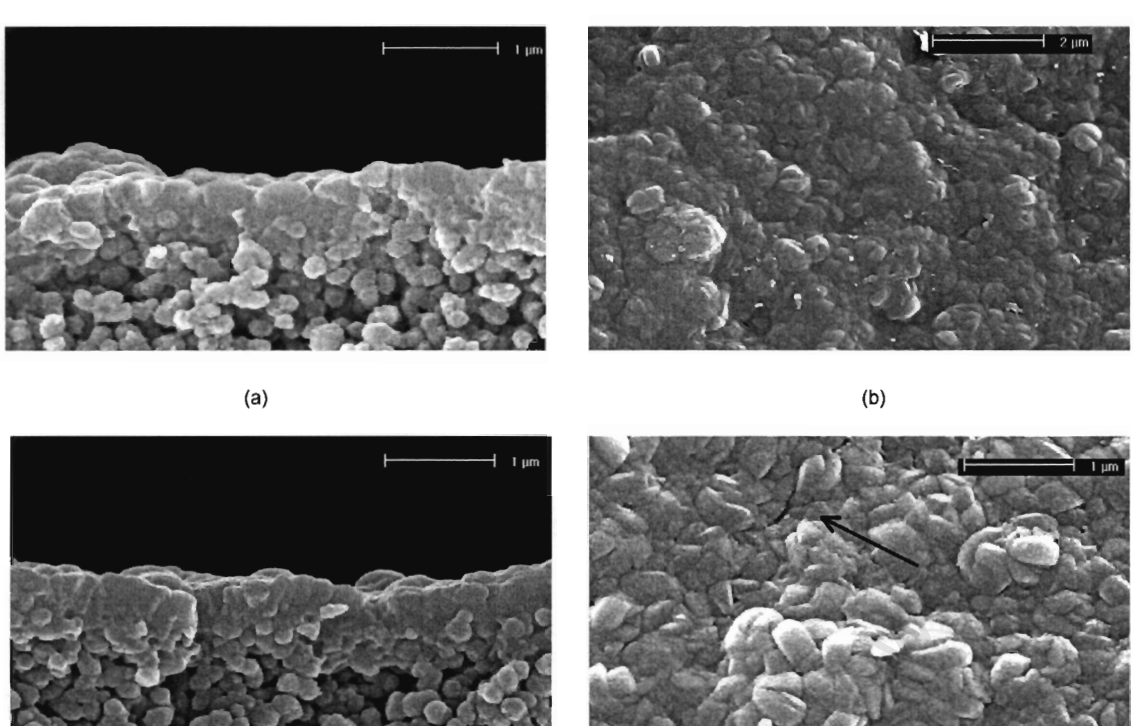

Figure 6.2: SEM images of membranes synthesised in the presence of structure directing agent, (a) side (b) top views of S2 membrane synthesis at 100°C for 36 hours, (c) side and (d) top views of Z1 membrane synthesised at 100°C for 27 hours.

sisted membranes. These well-defined crystals are as a result of competitive growth. Therefore crystals have a preferred orientation. XRD diffractograms can be used to determine the orientation of the zeolite membranes as will be discussed in the next section.

Figure 6.4(a) and (b) represent side and top images of the ZTF3 from the first batch of template free membranes synthesised respectively. Membranes from the first batch showed high permeance and poor selectivity, although these membranes were significantly thicker than the other membranes. Hence, SEM images were captured after single gas measurements. As can be seen in figure 6.4(a), a non-closed film has formed with large crystals of about 2-3 μm, scattered on the support surface, figure 6.4(b).

The non-closed films are believed to be due to the seeds becoming detached during calcination of the supports. The supports are calcined prior to synthesis, in order to remove any template in the seeds. However, the seeds are only attached electrostatically. During calcination at 500°C it appears that the seeds become

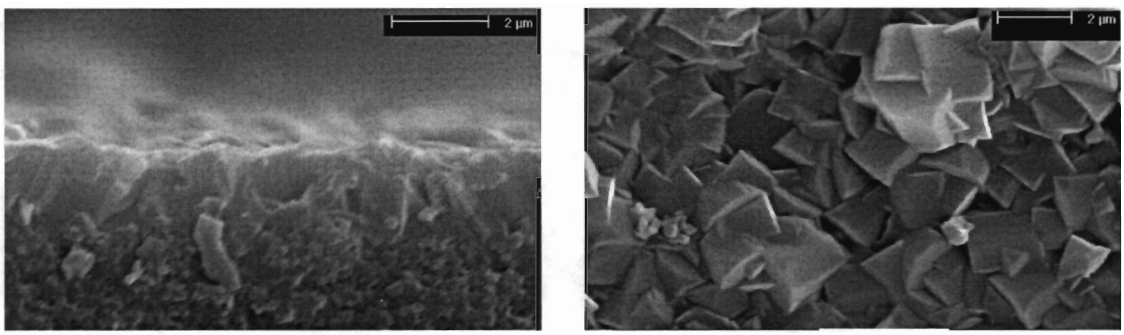

(a) (b)

Figure 6.3: SEM images of ZTF4 synthesised in the absence of structure directing agent, (a) side (b) top views of membrane synthesis at 180°C for 12 hours.

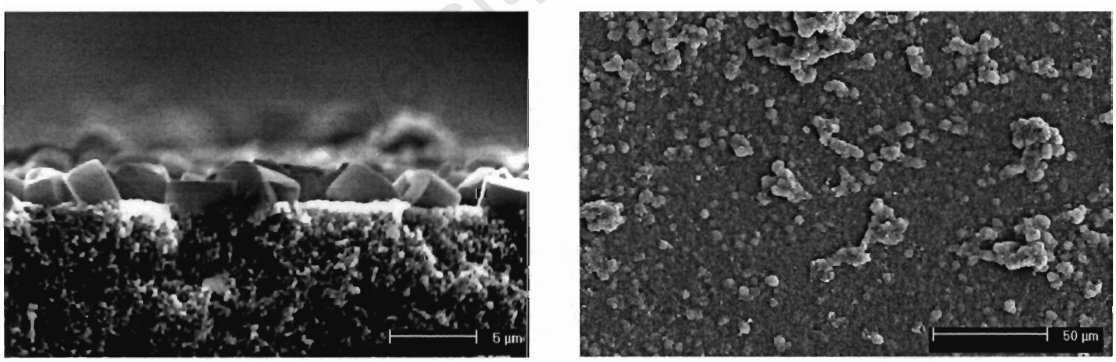

(a) (b)

Figure 6.4: SEM images of ZTF3 synthesised in the absence of structure directing agent and seeded support calcined, (a) side (b) top views of membrane synthesis at 180°C for 12 hours.

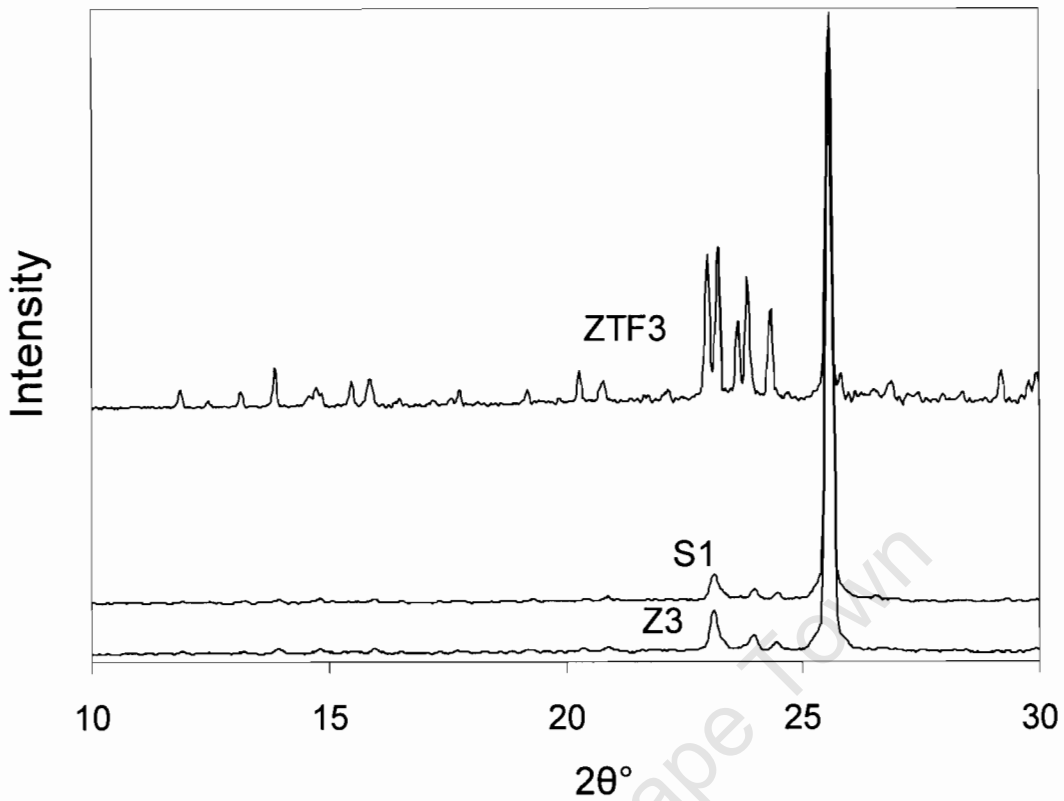

Figure 6.5: XRD analysis for S1, S2 and ZTF3 zeolite membranes.

detached from the support. To ensure that seeds are still attached to the support during synthesis, the supports were not calcined prior to synthesis. Hence zeolite pores will be blocked by template in the seeds. The template free membranes could not be calcined after synthesis as these membranes are not thermally stable enough to be heated to 500°C. Lassinantti *et al.* (2001) studied the temperature stability of these template free membranes by SF_6 permeance and SEM and concluded that the membranes are not stable above 250°C, at which point large cracks are formed. As the template free membranes have to be synthesised at 180°C, they can not be masked (wax used has a melting point of 120°C). Therefore there is considerable zeolite growth into the support and cracks may be formed during heating/ cooling, due to the differences in thermal expansion coefficients of zeolite and support.

6.1.2 X-ray Diffraction

XRD scans in figure 6.5 show that synthesised zeolite membranes are all crystalline and have MFI type structure, with the peak at 26° from the α-alumina support.

Table 6.1: Defect widths at varying relative partial pressures of n-hexane, Jareman et al., (2004)

P/P_0	Defect width (nm)	Equation applied
0.01	1.0	Horvath-Kawazoe
0.03	1.3	Horvath-Kawazoe
0.25	2.6	Kelvin
0.85	9.2	Kelvin
0.99	100	Kelvin

Peak intensities of the ZTF3 are much higher as this membrane is much thicker and contains three times as much zeolite. Further more, several groups have determined crystal orientation of the zeolite membranes by comparing XRD patterns of zeolite membranes to powders (assumed to have random orientation). By comparing the relative peak intensities, the zeolite axis orientation can be calculate. For template free membranes synthesised by the same procedure, Mintova *et al.* (1998) report that crystals are orientated with the c-axis inclined at 35° with respect to the support. Hedlund *et al.* (2003) report that membranes synthesised in the presence of structure directing agents are very weakly orientated with the a-axis perpendicular to the support. When the XRD scans in figure 6.5 are compared to membranes synthesised by Mintova *et al.* and Hedlund *et al.*, the template free membranes synthesised are orientated with the c-axis inclined at 35° with respect to the support. Membranes synthesised in the presence of a template are very weakly a-axis orientated.

6.1.3 n-hexane porosimetry

The permeance of helium was measured as a function of the relative partial pressure of n-hexane at room temperature. Table 6.1 shows the range of relative partial pressures used. With an increase in the relative partial pressure of n-hexane, pores of a certain diameter are blocked by the adsorbing species. According to the sizes indicated in table 6.1 this blockage results in a decrease in the helium permeance. Defect widths have been calculated at varying relative pressures of n-hexane using the Horvath-Kawazoe equation for defects <2 nm and the Kelvin equation for pores >2 nm (Jareman *et al.* 2004). For the dry helium, no pores are blocked, hence the permeance of helium is high. With the introduction of n-hexane ($P/P_0 \approx 0.01$), all zeolite pores and defects smaller than 1.0 nm will be blocked. The remaining flow of helium is via defects >1.0 nm. Progressively increasing the relative partial pressure of n-hexane, larger pores are blocked.

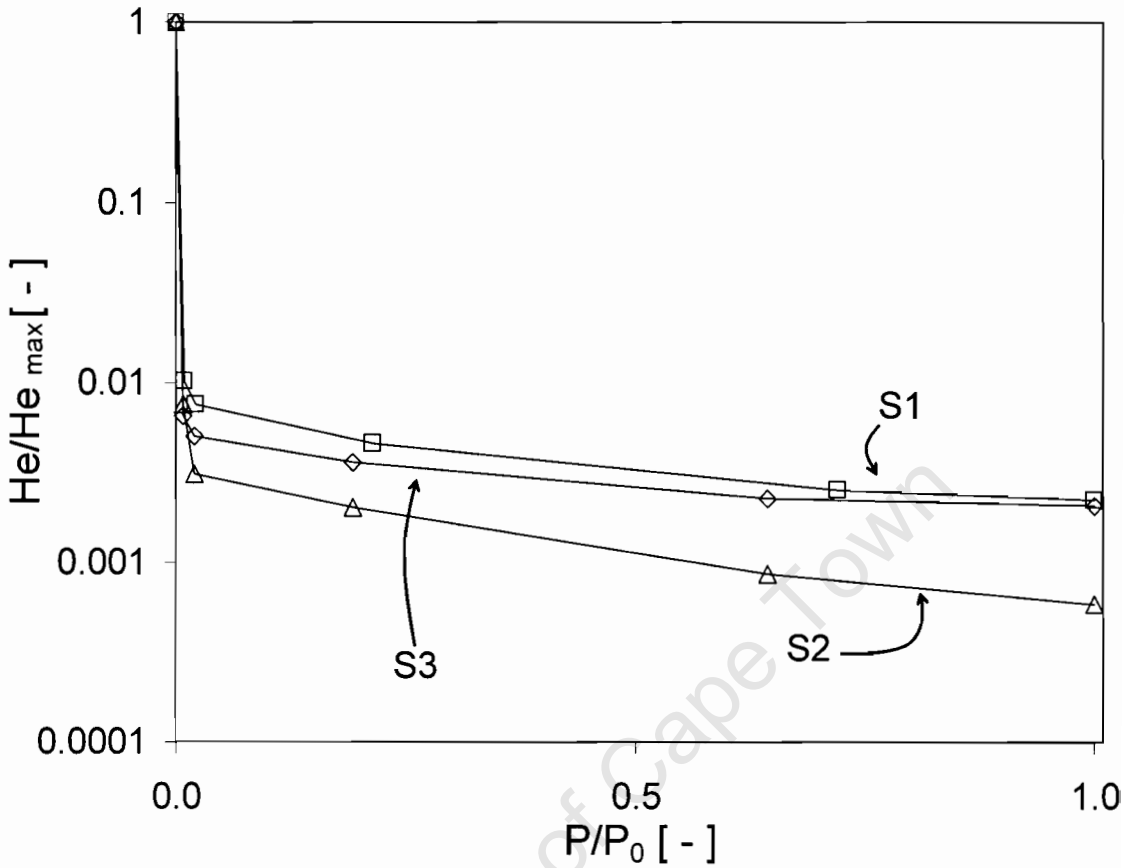

Figure 6.6: Relative helium permeance as a function of relative partial pressure of n-hexane, for silicalite-1 membranes.

Figures 6.6 and 6.7 show results for porosimetry measurements. As can be seen, the initial permeance for all silicalite-1 membranes is high in the absence of n-hexane, but with the introduction of n-hexane ($P/P_0 \approx 0.01$) the measured helium permeance has decreased by > 99%. Hence all silicalite membranes are high quality as >99% of the helium flow is via zeolite pores. All ZSM-5 membranes also have a high initial helium permeance. Z3 has an approximately 20% higher initial helium permeance than the other ZSM-5 membranes (table D.1, Appendix D). At n-hexane $P/P_0 \approx 0.01$ Z1 and Z2 show a permeance decrease by >99% hence these are also high quality membranes. However, Z3 shows approximately 70% decrease in permeance. Even at n-hexane $P/P_0 \approx 0.99$, about 25% of the initial flow remains. Therefore 25% of the flow through Z3 is via defects >100 nm, hence this membrane is not of high quality.

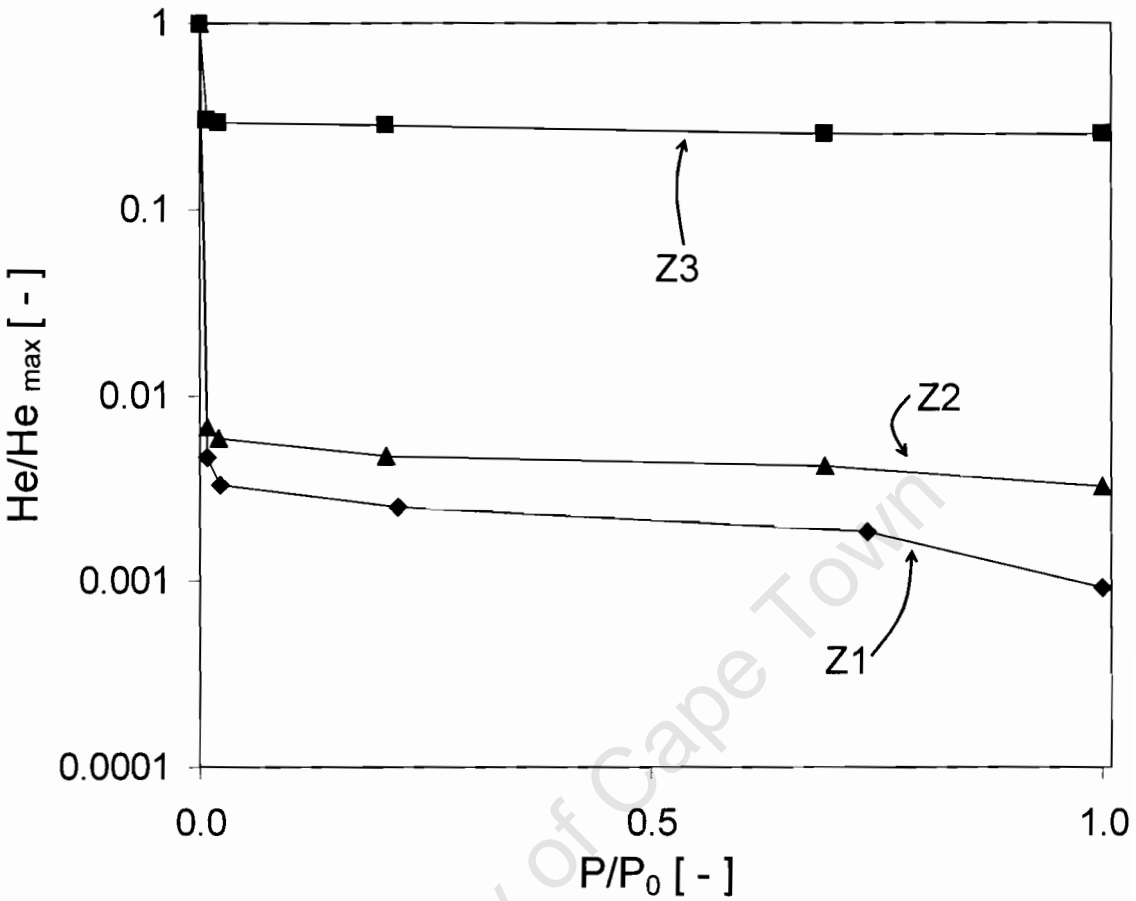

Figure 6.7: Relative helium permeance as a function of relative partial pressure of n-hexane, for ZSM-5 membranes.

6.2 Single gas permeance

Single gas measurements were carried out on blank supports, S1-S3 and Z1-Z3.

6.2.1 Analysis of support permeance

As the zeolite membranes are very thin, support contributions may be significant. Hence single gas permeance experiments were carried out on a blank support, in order to evaluate its effect. Table 6.2 shows pressure difference across the support and zeolite films. For a given flux the pressure difference was measured on the support and on the composite zeolite membrane. The contribution to pressure drop of the support across the membrane was then calculated (figure D.1, Appendix D). The resistance to flow through the support is as high as 48% for CO_2 hence viscous

Table 6.2: Analysis of the pressure drop across support and zeolite film for S2 at 25°C

Species	$\Delta P_{Support}$ [kPa]	$\Delta P_{Zeolite}$ [kPa]	ΔP_{Total} [kPa]	% Support
H_2	35	65	100	35
He	25	85	110	23
CO_2	55	60	115	48
SF_6	10	100	110	9.1

flow in the support is dominant. For SF_6 permeance the support contribution to the total pressure difference is 9% which is less significant. The differences in contribution of support are due to molecular mass and size of permeating species. For example, H_2 which is a small molecule has a large support contribution as its flux through the zeolite film is high. SF_6 which is a large molecule has a lower flux and in the zeolite film hence its' support contribution is small.

Figure 6.8 shows a plot of the linearised form of equation 5.3 for a blank support. Flux of each species was measured at 0.3 bar trans-membrane pressure difference, from 25°C to 300°C. Higher trans-membrane pressure differences could not be applied as the flux of species was greater than 1000 ml/min and could not be measured accurately. Equation 5.2 predicts that the flux (J_i) decreases with increasing temperature at constant ΔP. As can be seen from figure 6.8 all data fits this model well. For viscous flow the flux is a function of viscosity (equation 5.4). As the viscosity of gases increases with increasing temperature, the resistance to flow increases resulting in a reduced flux. The model fit means that within the support there is a combination of knudsen and viscous flow. Flux increases from SF_6 to H_2, i.e. with reducing molecular weight, as expected for both viscous and knudsen flow. From equation 5.3, the gradient of figure 6.8 gives viscous flow contribution and the intercept gives knudsen flow contribution. The ratio of the gradient to the intercept gives the dominant mechanism. Table D.2 (Appendix D) shows that viscous flow is the dominating mechanism of transport in the support. The model fit indicates that the permeance through the support may be described by a combination of knudsen diffusion and viscous flow acting in parallel. With increasing molecular mass and size knudsen flow becomes more significant. The ratio of viscous over knudsen mechanisms for H_2 $\approx$1200 whereas for SF_6 $\approx$100 indicating that even for SF_6 viscous flow contributes $>$ 99% to the mechanism of flow.

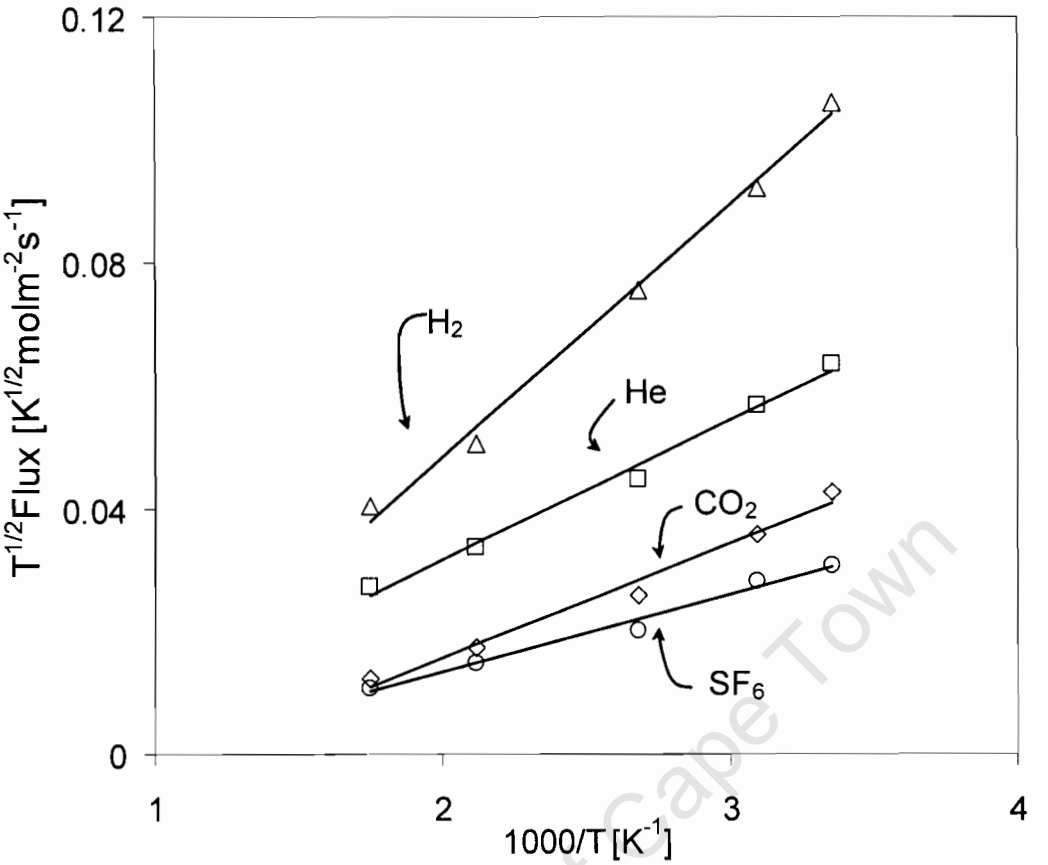

Figure 6.8: Effect of temperature on the flux for blank support at constant trans-membrane ΔP=0.3 bar.

6.2.2 Analysis of zeolite membrane permeance

The flowrate of each species was measured on the zeolite membranes at 25°C varying the trans-membrane pressure. Figure 6.9 represents B as a function of mean pressure across the membrane a silicalite-1 membrane at 25°C, from equation 5.2 for combined knudsen and viscous flow. The flow of all species has reduced in the zeolite membrane as compared to the support (tables D.8 and D.10, Appendix D). H_2 and He trends fits the model, equation 5.2. Therefore knudsen and viscous flow dominate the separation process in the zeolite membrane. The model (dashed lines) does not apply to CO_2 and SF_6. This is due to adsorption and large molecular size of these species. Helium permeance through the silicalite-1 membrane is much lower than CO_2 whereas for the blank support this was reversed.

Table 6.3 shows single gas permeance measurements for S2 and Z1 at 25°C and the percent difference between the flux of the two membranes. Although the

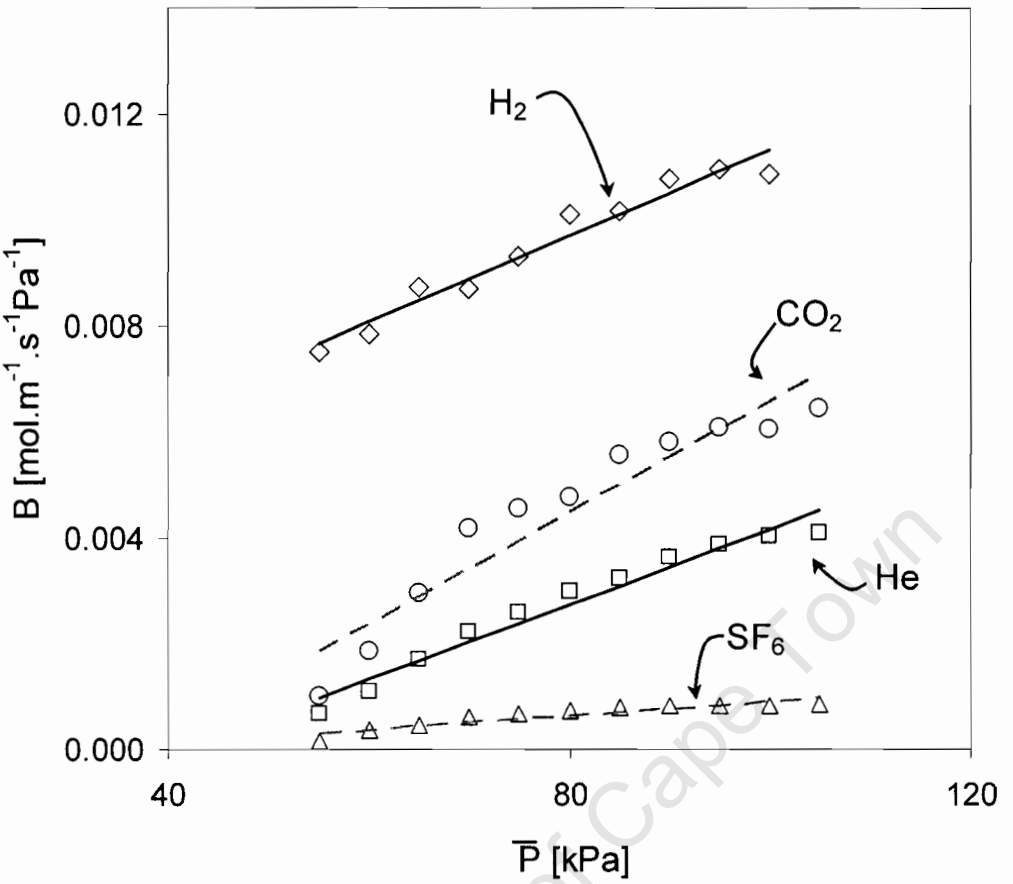

Figure 6.9: B (sum of viscous and knudsen parameters) of H_2, CO_2, He, and SF_6 as a function of mean pressure across the membrane for S2.

micro-structures of the two sets of membranes are identical all species have a lower permeance in ZSM-5 membranes other than CO_2. ZSM-5 membranes show approximately 25% lower hydrogen and helium permeance than the silicalite-1 membranes. This may be due to differences in mass transfer properties within the pores of each zeolite. Na^+ counter ions are present in the framework of ZSM-5 films as a result of charge balancing of the aluminium. This would result in narrowing of pores which could result in an increased resistance to diffusion. SF_6 permeance is reduced by about 50% as the large SF_6 molecule (5.5 Å, table 2.1), is more strongly affected by cations in ZSM-5. In the case of CO_2, a 7% increase in permeance is observed for the ZSM-5 samples. It has been suggested that Na^+ ions can act as sorption and transport sites for polar/polarisable molecules (Gora *et al.*, 2004) hence explaining the higher permeance of these species on ZSM-5. The same argument can be applied to N_2.

Table 6.3: The single gas permeance of S2 and Z1 at 25°C and trans-membrane pressure difference = 1bar

Species	Permeance [10^{-7}mol.m^{-2}.s^{-1}.Pa^{-1}]		%Δ(S2−Z1)
	S2	Z1	
H_2	212	162	24
N_2	124	105	15
He	77	57	26
SF_6	16	7.8	51
CO_2	118	126	-6.8

Table 6.4: Single gas ideal perm-selectivity at 25°C for S1-S2 and Z1-Z2 at trans-membrane pressure difference =1 bar

Selectivity	Membrane				Knudsen
	S1	S2	Z1	Z2	selectivity
N_2/H_2	0.59	0.59	0.65	0.68	0.27
He/H_2	0.39	0.36	0.35	0.37	0.71
SF_6/H_2	0.079	0.078	0.049	0.049	0.12
CO_2/H_2	0.56	0.51	0.78	0.82	0.21

Table 6.4 shows ideal perm-selectivities for S1-S2 and Z1-Z2, and the knudsen selectivities calculated from equation 2.11. It should be noted that any quality assessment, using single gas permeance ratios, may only be compared within each structure (i.e. silicalite-1 or ZSM-5) since the aluminium and the counter ions may influence the mass transfer properties. A detailed study was presented regarding this issue (Jareman and Hedlund, 2005). The He/H_2 perm-selectivity does not vary from silicalite-1 to ZSM-5; however SF_6/H_2 perm-selectivity is much lower for ZSM-5 membranes. Again the explanation would be a result of obstruction of SF_6 molecule due to its bulk and size in ZSM-5 compared to silicalite-1 membranes. The support contribution for SF_6 is about 9%. This explains why the measured SF_6/H_2 selectivity, table 6.4, was better than that kundsen selectivity calculated from equation 2.11. Single gas permeance ratios for the prepared membranes in table 6.4 compare well with results by Hedlund *et al.* (2003).

Comparing helium single gas permeance results to calculated knudsen selectivities, it appears as if the dominating transport mechanism is not that of the zeolite film. Measured selectivities are lower than the respective knudsen selectivities. Although these perm-selectivities cannot be directly related to knudsen selectivity, they indicate that permeance may be due to viscous flow as a result the pressure difference. The resistance to mass transfer of the zeolite film is low, as the films are only 500 nm thick, the separation selectivity is not controlled by the zeolite film

layer. Measured SF_6/H_2 perm-selectivity is significantly lower than that calculated by knudsen selectivity. Due to the larger size and lower flux of this species across the membrane, separation in the zeolite layer dominates.

6.3 Mixture separations

The helium sweep gas will have a partial pressure gradient across the membrane opposing that of hydrogen and water. This is common in literature where a sweep gas is used, but is almost always neglected. The back diffusion of helium may reduce the permeance of hydrogen. In order to minimize this effect, helium was used as the carrier for water. By doing so the driving force for back diffusion is reduced. The actual helium permeance could not be measured as GC detection was not possible since the GC carrier gas was also helium. In the following sections helium is assumed to act only as a solvent and its permeance across the membrane has been neglected. There is no pressure difference across the membrane and thus no viscous flow for all species during mixture separations.

6.3.1 Binary mixture separations

Binary H_2O/H_2 mixture separations where carried out on S2, S3, Z1, Z2, ZTF1-5, and ZTF6.

Membranes prepared using templates

Figure 6.10 shows mixture permeance of water and hydrogen for the same silicalite-1 and ZSM-5 membranes respectively. At 25°C water permeance is 18.8×10^{-7} and 29.9×10^{-7} for silicalite-1 and ZSM-5 membranes respectively and hydrogen permeance is 2.7×10^{-7} and 1.3×10^{-7} $mol.m^{-2}.s^{-1}.Pa^{-1}$ for silicalite-1 and ZSM-5 membranes respectively. The hydrogen permeance in the binary system is two orders of magnitude lower than that of pure component permeance at 25°C. This is due to the presence of H_2O, which adsorbs onto zeolite and blocks the pores. At 25°C H_2O, adsorbs strongly in the pores essentially filling them, while H_2 adsorption is essentially negligible. H_2 is dragged through the membrane by the surface diffusion of water. Hydrogen permeance is two orders of magnitude lower than in single gas measurements, flow is not in the knudsen regime.

With increasing temperature, H_2 permeance increases rapidly as a result of the desorption of water. The hydrogen permeance increases to about 18×10^{-7}

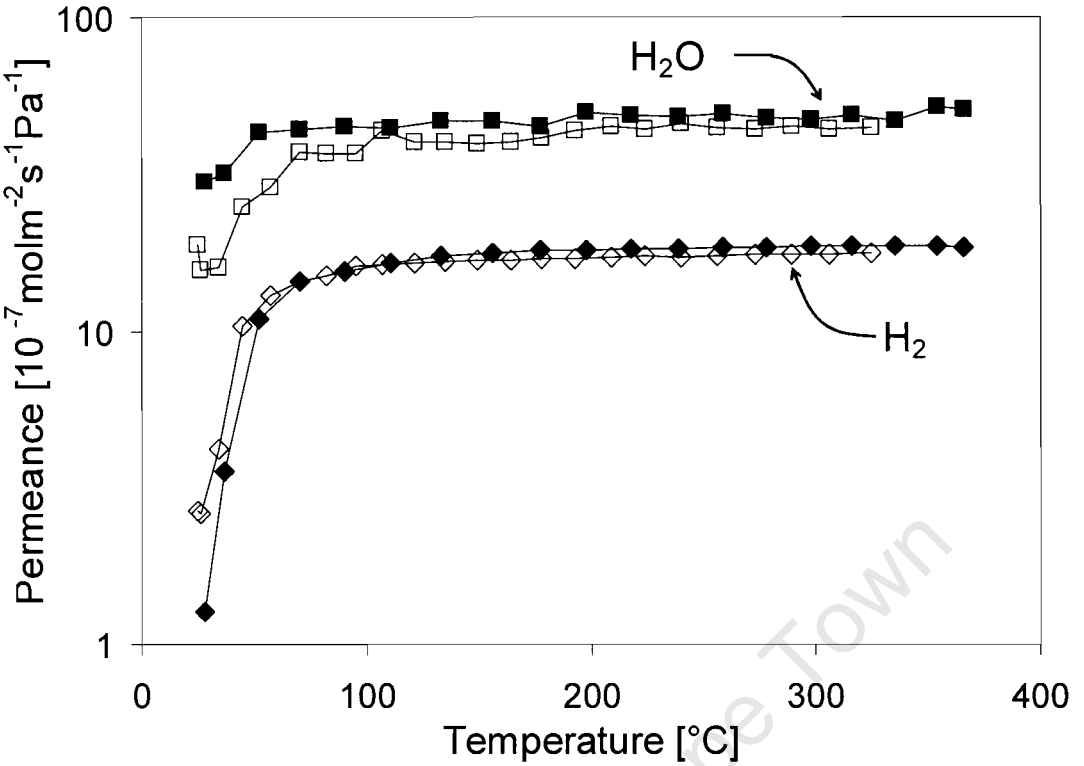

Figure 6.10: Binary species permeance as a function of temperature using a mixture of 20 kPa H_2, 1.9 kPa H_2O, in a He carrier for S3 (open symbols) and Z1 (filled symbols) membranes.

$mol.m^{-2}.s^{-1}.Pa^{-1}$ for both membranes above 150°C. H_2O permeance reaches a maximum of 45×10^{-7} and 50×10^{-7} $mol.m^{-2}.s^{-1}.Pa^{-1}$ for silicalite-1 and ZSM-5 membranes respectively. The difference in permeance for the two membranes may be due to higher sorption capacity of ZSM-5 membranes for water, aiding surface diffusion even at higher temperatures. This would not affect hydrogen as it essentially does not adsorb onto the membranes at the given pressures. The permeance of hydrogen is similar for both membranes.

Figure 6.11 shows binary H_2O/H_2 separation selectivity for silicalite-1 and ZSM-5 membranes as a function of temperature. In both cases the selectivity decreases with increasing temperature. This behaviour is expected. With increasing temperature, the adsorption of water is reduced hence more H_2 can permeate in much the same way as in n-hexane porosimetry. However, the ZSM-5 membrane selectivity is 10.4 at 25 °C, compared to 4.3 for the silicalite-1 membrane. The higher selectivity of ZSM-5 membranes is due to the hydrophilic character of these membrane, compared to the silicalite-1 membrane. At temperatures exceeding 70°C the separation

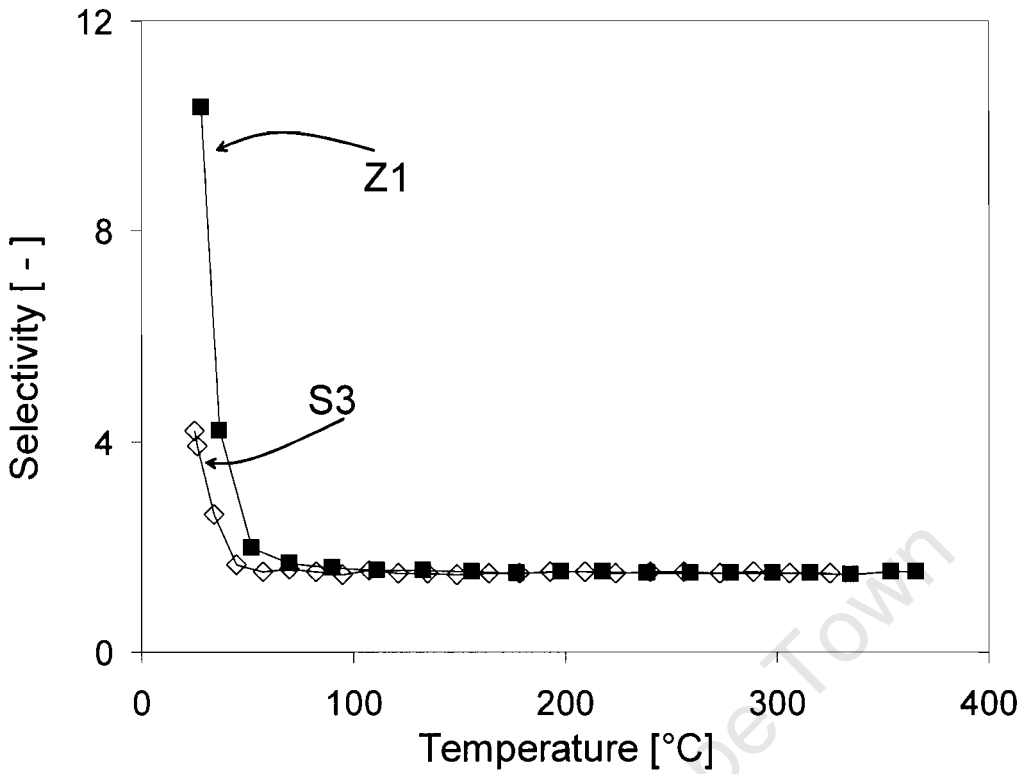

Figure 6.11: Binary H_2O/H_2 separation selectivity as a function of temperature using a mixture of 20 kPa H_2, 1.9 kPa H_2O, in a He carrier for S3 and Z1 membranes

selectivity of both membranes was similar at about 1.4-1.5. The knudsen selectivity for H_2O/H_2 is 0.33, equation 2.11. Measured selectivities are higher than knudsen selectivity, indicating that the dominant mechanism of flow is adsorption-surface diffusion.

Membranes prepared without template

Figure 6.12 shows binary H_2O/H_2 permeance and separation selectivity for template free ZSM-5 membranes as a function of temperature. H_2 and H_2O permeance are 0.3×10^{-7} and 14.3×10^{-7} mol.m^{-2}.s^{-1}.Pa^{-1} at 25°C increasing to 0.9×10^{-7} and 20.1×10^{-7} mol.m^{-2}.s^{-1}.Pa^{-1} at 120°C. Both species permeances are significantly lower than the membranes synthesised using a template. The lower fluxes would also be as a result of increased mass transfer resistance and pore blockage. Template free zeolite films are 3 times thicker and the template remains in the seeds. Seed crystals are 60 nm spheres and do not form a dense layer during seeding. Therefore permeance can occurs through MFI pores around these seeds. The orientation with

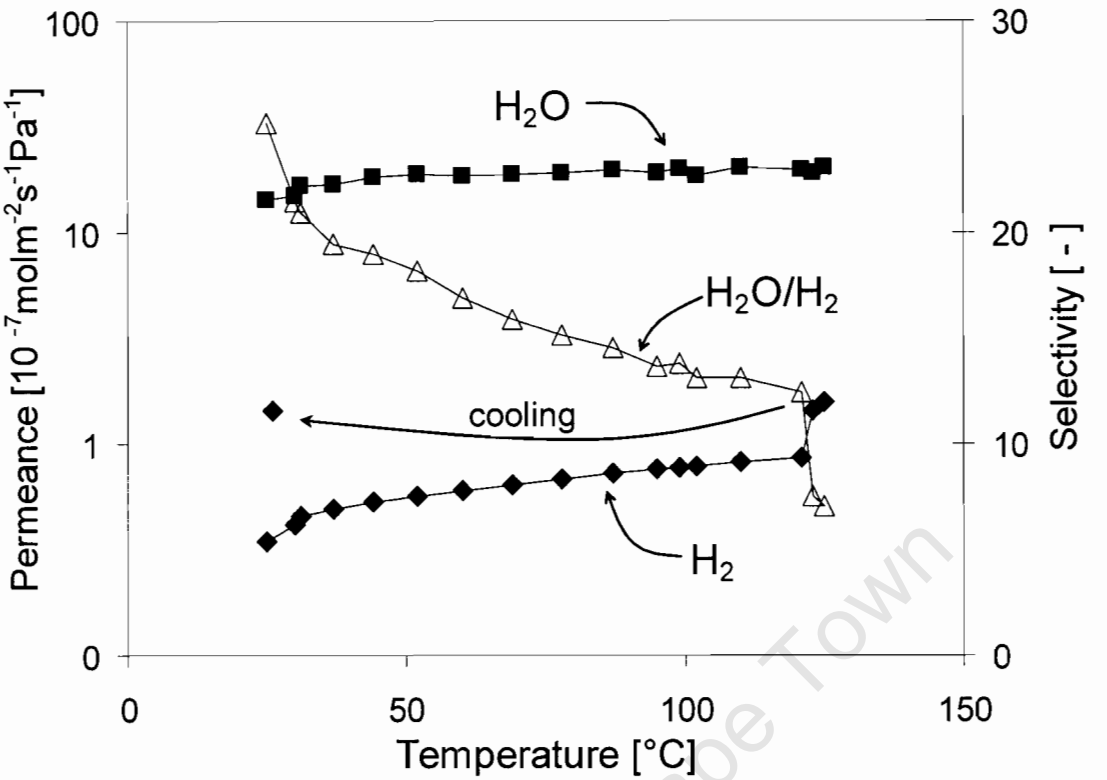

Figure 6.12: Binary separation selectivity and species permeance as a function of temperature for ZTF6 using a mixture of 20 kPa H_2, 1.9 kPa H_2O, in a helium carrier.

the c-axis inclined at 35° with respect to the support means that zeolite tortuosity increases, contributing to the lower permeances.

At 25 °C, the selectivity for the 1600 nm thick template free ZSM-5 membranes is 25.1 as compared to 10.4 and 4.3 for the 500 nm silicalite-1 and ZSM-5 membranes. The template free membranes are much more hydrophilic and water is adsorbed more strongly in these membranes. With increasing temperature selectivity to water decreases. However, ZTF6 selectivity decreases much more slowly than the S3 and Z1. At 100°C, selectivity for S3 and Z1 is approximately 1.5 and has levelled off whereas it is 13.1 for the template free membranes and still decreasing. The higher selectivity of the membranes may be due to a reduced accessibility to the zeolite pores by hydrogen due to the orientation of the films. For xylene isomer separations Lai *et al.* (2003) investigated the effects of crystal orientation. They conclude membranes with b and c-axis crystal orientated perpendicular to support can be 2 to 3 orders of magnitude more selective than non/weakly orientated crystals. Hence crystal orientation may also explain increased and maintained selectivity in

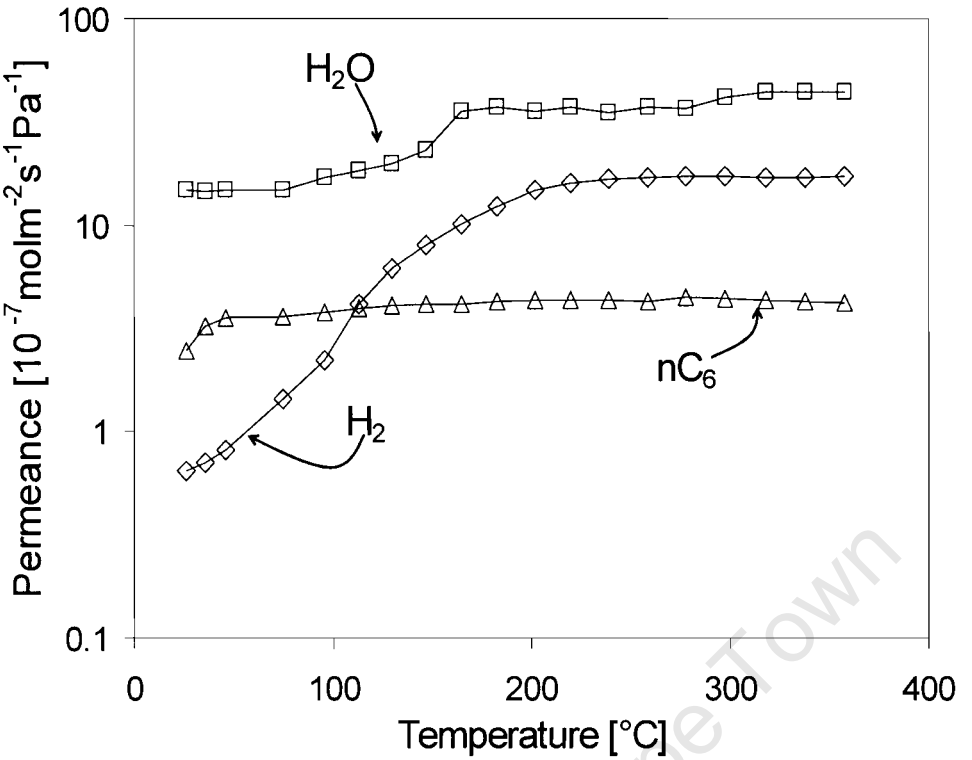

Figure 6.13: Ternary species permeance as a function of temperature for S3 using a mixture of 19 kPa H_2, 1.8 kPa H_2O, 3.7 kPa nC_6, in a helium carrier.

this case.

Above 120°C it was observed that there was a sudden increase in the permeance of hydrogen, and a decrease in selectivity indicating that the membrane may have formed defects, most likely cracks due to the thermal treatment. The membrane was cooled down and more separations experiments carried out. At 25°C the permeance of hydrogen now remained similar to that prior to cooling, indicating that the membrane had in fact developed cracks. As was discussed earlier reproducibility and stability of the template free membranes is of concern and must be improved in future work.

6.3.2 Ternary mixture separations

Figures 6.13 and 6.14 show ternary species permeance for silicalite-1 and ZSM-5 membranes as a function of temperature. At 25°C the permeance of water in the ternary mixture is lower compared to the binary mixture. The permeance of water in the ternary mixture is 14.8×10^{-7} and 15.6×10^{-7} as compared to 18.8×10^{-7} and

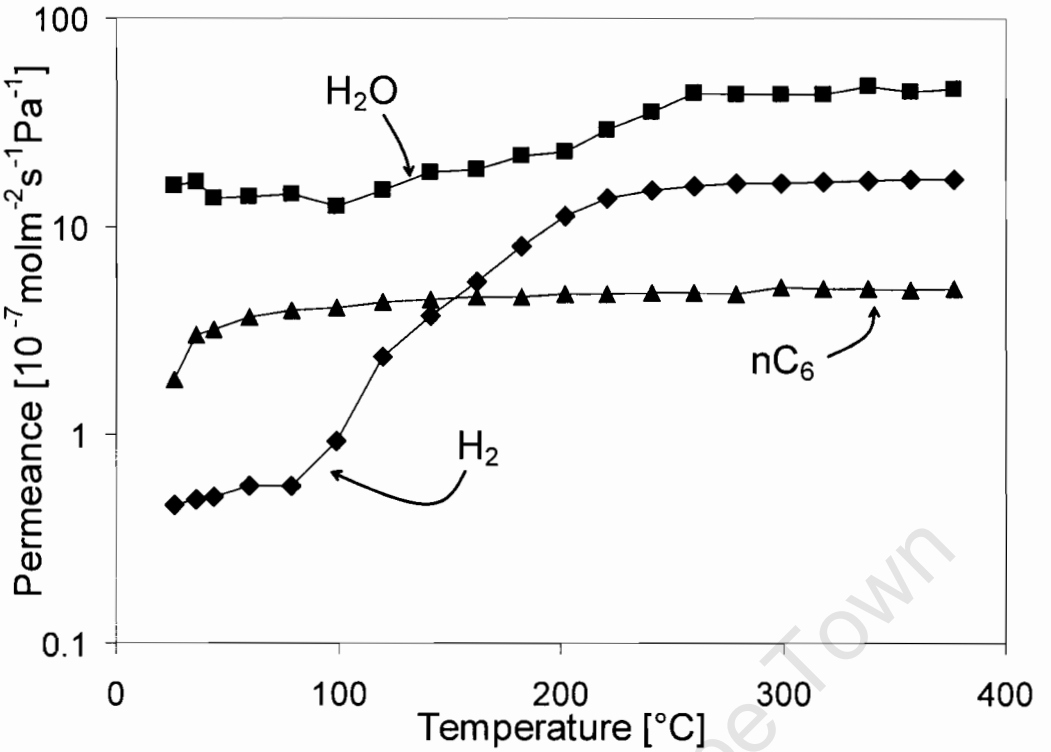

Figure 6.14: Ternary species permeance as a function of temperature for Z1 using a mixture of 19 kPa H_2, 1.8 kPa H_2O, 3.7 kPa nC_6, in a helium carrier.

29.9×10^{-7} mol.m^{-2}.s^{-1}.Pa^{-1} for the binary mixture for S3 and Z1 respectively. The decrease may be due to competitive adsorption of n-hexane which displaces some of the water. Above 200°C the water permeance is similar to binary permeance of both silicalite-1 and ZSM-5 membranes, approximately 45×10^{-7} mol.m^{-2}.s^{-1}.Pa^{-1}. The permeance of hydrogen is 0.6×10^{-7} and 0.5×10^{-7} mol.m^{-2}.s^{-1}.Pa^{-1} at 25°C, for silicalite-1 and ZSM-5 membranes respectively and it is constant above 250°C at approximately 17×10^{-7} mol.m^{-2}.s^{-1}.Pa^{-1}, similar to that of binary mixtures.

Figure 6.15 shows ternary H_2/H_2O and H_2O/nC_6 separations selectivity for silicalite-1 and ZSM-5 membranes as a function of temperature. Both membranes show similar separation selectivity trends. With the addition of a third species, n-hexane, an increase in selectivity for both membranes is observed at 25°C compared to binary separations. For the silicalite-1 membrane the H_2O/H_2 selectivity increases from 4.3 in the binary mixture to 14.8 in the ternary mixture. H_2O/H_2 selectivity for the ZSM-5 membrane also increases from 10.4 in the binary mixture to 19.9 in the ternary mixture. Xomeritakis *et al.* (2001) also report increased selectivity in silicalite-1 membranes for xylene isomer separation with the addition

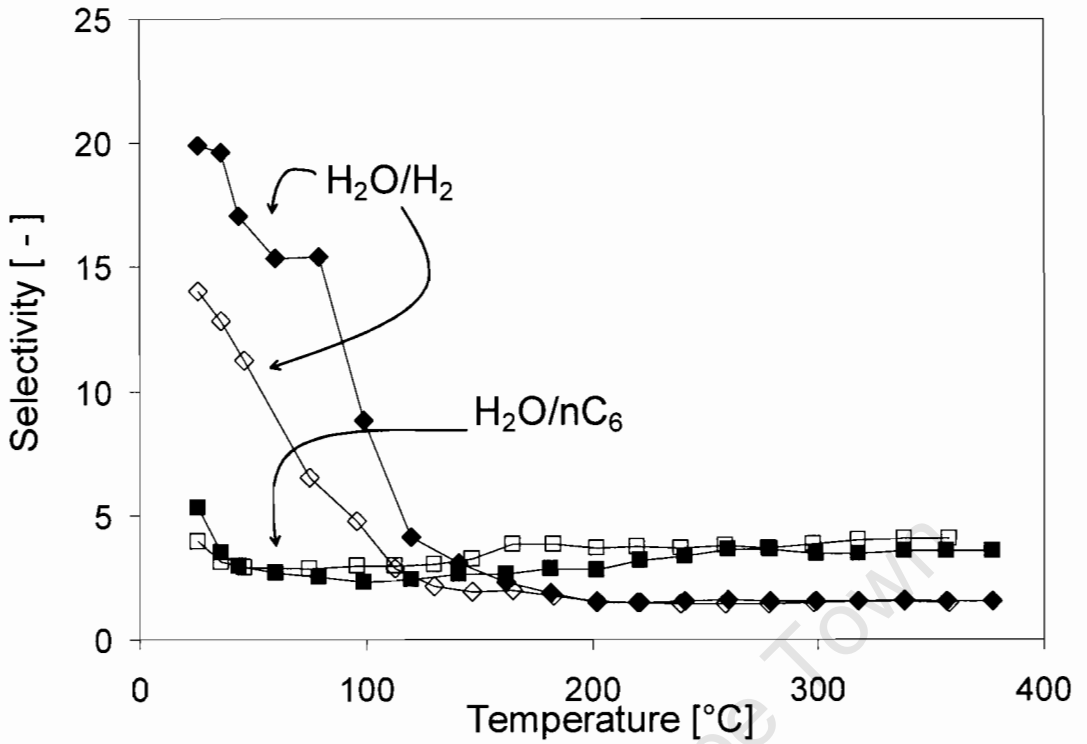

Figure 6.15: Ternary separations selectivity as a function of temperature for S3 (open symbols) and Z1 (filled symbols) using a mixture of 19 kPa H_2, 1.8 kPa H_2O, 3.7 kPa nC_6, in a helium carrier.

of n-hexane. The n-hexane adsorbs onto zeolitic pores, increasing pore occupancy. This reduces the flux of H_2 more than H_2O, as H_2 is does not adsorb onto the zeolite, thus increasing H_2O/H_2 selectivity. With increasing temperature the H_2O/H_2 selectivity tends to 1.5 for both membranes, approximately the same as that of the binary mixture. However, for the ternary mixture this decrease is much slower leveling off at about 200°C for both membranes. The H_2O/nC_6 selectivity trend of the two membranes is similar. At 25°C H_2O/nC_6 selectivity is 4.0 and 5.3 for silicalite-1 and ZSM-5 membranes respectively. The selectivity decreases with increasing temperature due to an increase in the water permeances while the n-hexane permeance remains constant for S3 and Z1 membranes respectively.

6.4 MS modelling of transport in membrane

Figures 6.16(a) and (b) shows the permeance as a function of temperature for the Maxwell-Stefan model developed from equations 5.5-5.14 and equations 2.9-

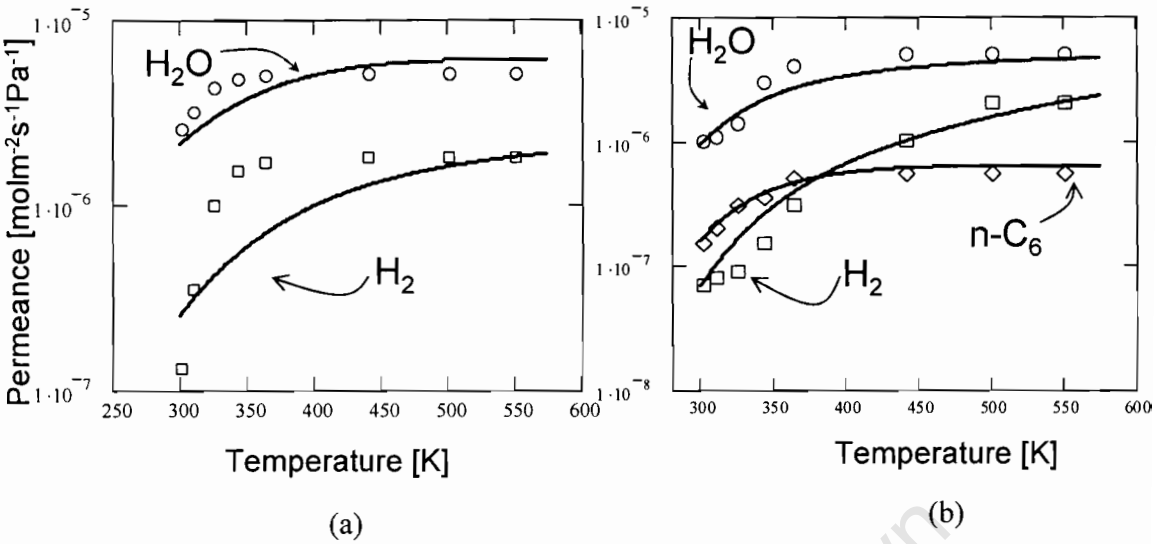

Figure 6.16: Showing permeance as a function of temperature for the Maxwell-Stefan equations, binary (a) and ternary (b) mixtures with experimental data from Z1.

2.8. Figure 6.16(a) shows binary hydrogen and water permeance and figure 6.16(b) ternary hydrogen, water and n-hexane permeance. It was assumed that partial pressure difference across the membrane is constant as a function of temperature for all species. Furthermore it is assumed that due to the presence of sweep gas the partial pressure of species on the permeate side is 1 Pa, i.e. the sweep gas removes the permeate as it appears, but not all the permeate is removed. Diffusion, and isotherm parameters were changed so as to fit experimental data (Appendix D). The values do not compare well with (Somers *et al.* 2003)

The MS model does not predict binary hydrogen permeance adequately. However, ternary hydrogen permeance is predicted more accurately. A possible explanation for the underestimation of the model compared to experimental data is that at 25°C water adsorption blocks zeolite and defective pores. Increasing temperature results in desorption of water, hence defects are no longer blocked and hydrogen permeance is higher than expected (since defects are not taken into account in the model) as it can now also permeate via defects. Figures E.1 and E.2 show the permeance of hydrogen as a function of relative partial pressure of water and n-hexane, (Appendix E). These are similar to the porosimetry plots. Figure 6.17(a)-(e) shows binary and ternary surface concentrations of species from the model. The surface concentration of n-hexane is high even at high temperatures, resulting in a higher pore occupancy and lower H_2 permeance. Therefore n-hexane blocks hydrogen per-

meance better than water. Comparison of figures 6.17(d) and (e) shows that at low temperatures water displaces n-hexane, but at higher temperature n-hexane displaces water on the surface of the zeolite. For the MS model with the addition of n-hexane the ternary hydrogen permeance is predicted more correctly. Water and n-hexane permeance is predicted well by the model.

The MS model developed does not take into account the presence of a support and its resistance to flow. This simplification may be reasonable for mixture separations as the flux of H_2 has reduced by two orders of magnitude as compared to single gas permeation where the support contribution can not be neglected due to the high flux through the zeolite film. Deviations of the model may also be due to use of the He as the solvent for water and sweep gas which has been neglected in the model.

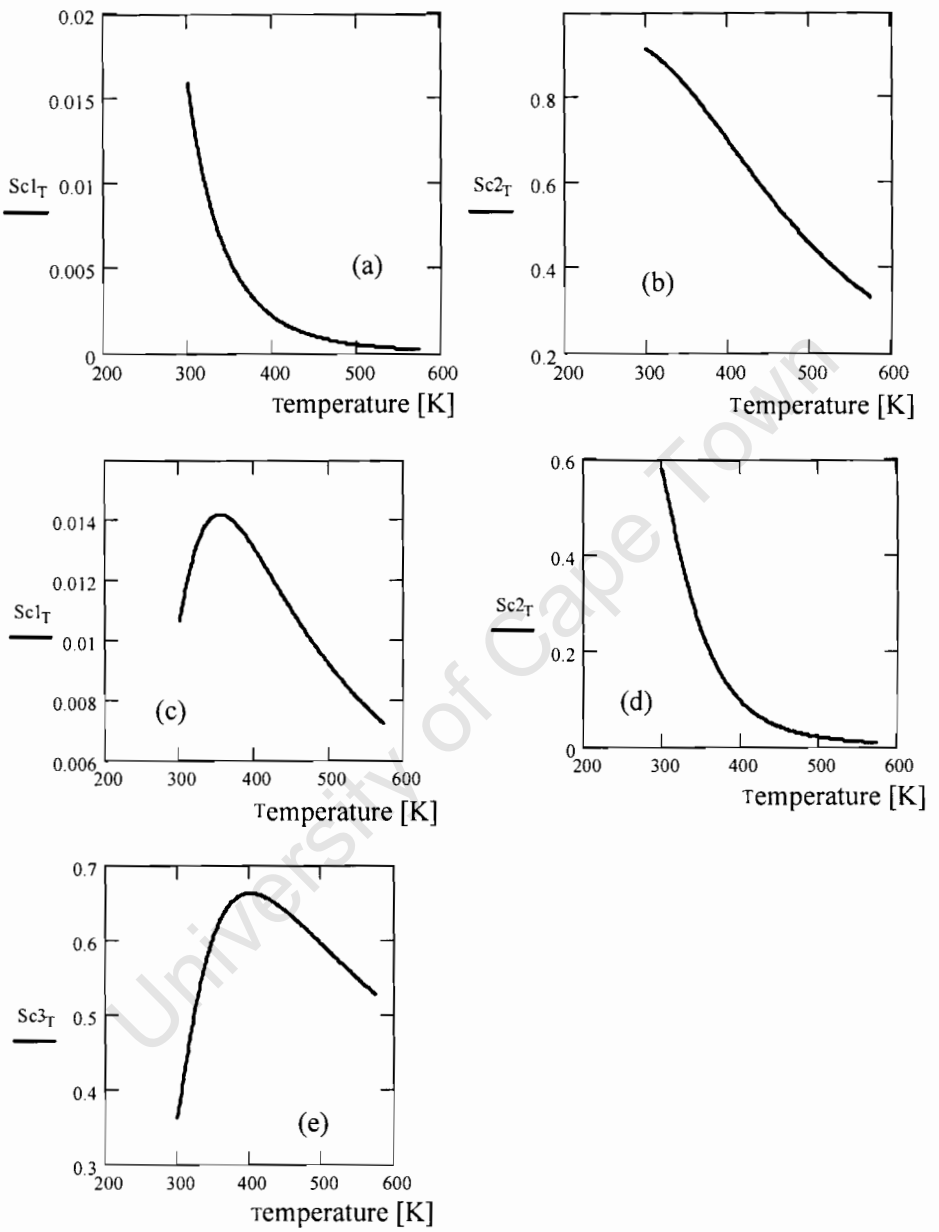

Figure 6.17: Surface concentration (mole fraction of species) of binary H_2(a), H_2O (b), and ternary H_2(c), H_2O (d), nC_6 (e) based on MS model.

Chapter 7

Conclusions

MFI zeolite membranes with varying Si/Al ratios were synthesised using two different synthesis procedures: with and without the aid of structure directing agents. The membranes were characterised by SEM, XRD and n-hexane porosimetry. Pure component flux was measured on blank substrate, silicalite-1 and ZSM-5 (Si/Al≈40) membranes. Binary H_2O/H_2 mixture separations were carried out on silicalite-1, ZSM-5 (Si/Al≈40) and template free membranes (Si/Al≈10). Ternary $H_2O/H_2/nC_6$ mixture separations were carried on silicalite-1 and ZSM-5 (Si/Al≈40) membranes.

From the comparison pure component support and composite zeolite membranes it can be concluded that the contribution of support to the total pressure difference is significant. Support contributions as high as 48% were calculated. This is due to the low resistance of the zeolite film, as they are very thin. However, in mixture separations, as the total flux of hydrogen has decreased by about two orders of magnitude, effects of the support are no longer significant. A single gas model for knudsen and viscous flow was developed. From the experimental data it is concluded that in most cases knudsen and viscous flow in the support are the dominating transport mechanisms in single component gas permeance.

Two membranes which differed only in the Si/Al content where compared. Results show that increasing the Al content H_2O/H_2 selectivity increases. The increase in selectivity is due to the stronger adsorption of water in ZSM-5 membranes. With the addition of n-hexane the H_2O/H_2 selectivity of both membranes increases. With an increase in temperature, selectivity decreases due to desorption of water.

Membranes synthesised by the template free technique cannot be compared to the ones synthesised in the presence of a template. Template free membranes are thicker and orientated. These membranes have a much higher selectivity compared to membranes synthesised with a template, which is due to the orientation of these

membranes.

For the separation of a mixture simplified Maxwell-Stefan equations were developed, using a multi-component langmuir adsorption model, to describe multi-component permeation. For binary mixtures the models adequately describe water permeation, however the calculated hydrogen flux significantly deviates from experimental flux. For ternary mixtures the model adequately describes permeation of all species.

Chapter 8

Recommendations

From the experimental and modelling work done in this thesis the following recommendations can be made for further work:

- Synthesis of membranes on supports with higher porosity to reduce support effects on the separation process,
- Ion-exchange of ZSM-5 membranes with larger cations to improve selectivity of membranes,
- Improve the synthesis technique for template free membranes for better reproducibility of results as these membranes showed much higher selectivity above 100°C,
- Implement the zeolite membranes tested in this work into membrane reactors for the in-situ removal of water from the Fischer-Tropsch Synthesis,
- The applied Maxwell-Stefan model for predicting multi-component species permeance can be further developed by considering finite interaction parameters, $Đ_{ij}$,
- More complex adsorption isotherm models that take into account the different saturation surface occupancy of species can be applied, and
- Measure water and n-hexane multi-component isotherms for application in the MS model.

References

Bernal M., Coronas J., Menéndez M. and Santamaría J., Coupling of reaction and separation at the microscopic level: esterification processes in a H-ZSM-5 membrane reactor, Chemical Engineering Science, 57, (2002), 1557-1562

Bowen T., Noble R., and Falconer J., Fundamentals and applications of pervaporation through zeolite membranes, Journal of Membrane Science, 245, 1 (2004) 1-33

Caro J., Zeolites and mesoporous materials as advanced functional materials Proceedings: 14th International Zeolite Conference, (2004), 1-8

Caro J., Noack M., Kölsch P., Schafer R., Zeolite membranes - state of their development and perspective, Microporous and Mesoporous Materials, 38, (2000), 3-24

Chaing A., and Chao K., Membranes and films of zeolites and zeolite like materials, Journal of Physics and Chemistry of Solids, 62, (2001), 1899- 1910

Clark T., Deckman H., Cox D., Chance R., In situ determination of adsorption of the characteristics of a zeolite membrane, Journal of Membrane Science 230, (2004), 91-98

Deckman H., Cox D., Bons A., Carstensen B., Chance R., Corcoran E., Gijnst W., McHenry J., Reinoso J., Saunders R., Tindall P., IWZMM2001 Book of Abstracts, (2001), 1- 9

Den Extre M., van Bekkum H., Rijn C., Kapteijn F., Moulijn F., Schellevis H. and Beenakker C., Stability of oriented silicalite-1 films in view to preparation, Zeolites, 19 (1), (1997), 13-20

Do D., Adsorption analysis: Equilibria and Kinetics, Imperial college press, (1998)

Espinoza, R., Du Toit E., Santamara J., Menendez M., Coronas J., and Irusta, S. (2000). Use of membranes in Fischer-Tropsch reactors Studies in Surface Science Catalysis, 130, 389-394

Funke H., Kovalich M., Falconer J., and Noble R., Separation of hydrocarbon isomer vapours with Silicalite Zeolite membranes, Industrial Engineering Chemistry 35, (5), (1996), 1575-1582

Gallucci F., Paturazo L., Basile A., An experimental study of CO_2 hydrogenation into methanol involving zeolite membranes reactor Journal of Chemical engineering and Processing, (43), (2004), 1029-1036

Gora L., van den Berg A., Zhu W., Jansen J., Kapteijn F., and Maschmeyer T., proceedings: 14th International Zeolite Conference, (2004), 612-619

Hedlund J., Noack M., Köisch P., Creaser D, Caro J., Sterte J., ZSM-5 membrane synthesis without organic template using a seeding technique, Journal of Membrane Science 159, (1999), 263-273

Hedlund J., Sterte J., Anthonis M., Bons A., Carstensen B., Corcoran N., Cox D., Deckman H., De Gijnst W., de Moor R., Lai F., McHenry J., Mortier W, Reinoso J., Peters J., High flux MFI membranes, Microporous and Mesoporous Materials, 52, (2002), 179-189

Hedlund J., Control of the preferred orientation in MFI films synthesized by seeding, Journal of Porous materials, 7 (2000) 455-464

Hedlund J., Jareman F., Bons A. and Anthonis M., A masking technique for high quality MFI membranes, Journal of Membrane Science, 222, 1-2, 1 (2003), 163-179

Hedlund J., Noack M., Köisch P., Creaser D., Caro J., Sterte J., ZSM-5 membrane synthesis without organic template using a seeding technique, Journal of Membrane Science 159, (1999), 263-273

Iglesia E., Design, Synthesis and use of a cobalt-based Fischer-Tropsch synthesis catalyst, Applied Catalysis A: General, 161, (1997), 59-78

Jacobs G., Das T., Patterson P., Li J., Sanchez L., Davis B., Fischer-Tropsch synthesis XAFS studies of the effect of water on a Pt-promoted Co/Al_2O_3 catalyst, Applied Catalysis A: General, 247, (2003), 335-343

Jareman F., Hedlund J., Creaser D. and Sterte J., Modelling of single gas permeation in real MFI membranes, Journal of Membrane Science, 236, (2004), 81-89

Jareman F. and Hedlund J., Permeation of H_2, N_2, He and SF_6 in real MFI membranes, Microporous and Mesoporous Materials, 82, (2005), 201–207

Jareman F., Andersson C., and Hedlund J., The influence of the calcination rate on silicalite-1 membranes, Microporous and Mesoporous Materials, 79, (2005), 1-5

Kapteijn F., Bakke W., J can de Graff, Zheng G., Poppe J. and Moulijn J., Permeation and separation behaviour of a silicalite-1 membrane, Catalysis Today, 25, (3-4), (1995), 213-218

Kärger J. and Ruthven D., Diffusion in zeolites and other microporous solids, Wiely and Sons Inc, (1992)

Krishnamoorthy S., Tu M., Ojeda M., Pinna D., and Iglesia E., An investigation of the Effects of water on Rate and Selectivity of the Fischer-Tropsch Synthesis on Cobalt-Based Catalysts, Journal of Catalysis, 211 (2002) 422-433

Krishna R. and Baur R., Analytic solution of the Maxwell-Stefan equations for multicomponent permeation across a zeolite membrane, Chemical Engineering Journal, 97, (2004), 37-45

Krishna R. and Baur R., Modelling issues in zeolite based separation processes, Separation and Purification Technology, 33, (2003), 213-254

Krishna R., Multicomponent surface diffusion of adsorbed species: A description based on the generalized Maxwell-Stefan equations, Chemical engineering science, 45, (1990), 1779-1791

Lai Z., Bonilla G., Diaz I., Nery J., Sujaoti K., Amat M., Kokkoli E., Terasaki O., Thompson R., Tsapatsis M., Vlachos D., Microstructural optimization of a zeolite membrane for organic vapour separation, Science, 300, (2003), 456

Li G., Kikuchi E., Matsukata M., Separation of water-acetic acid mixtures by pervaporation using thin mordenite membrane, Separation and Purification Technology 32 (2003), 199-206

Lassinantti M., Hedlund J., Sterte J., Faujasite-type films synthesized by seeding, Microporous and Mesoporous Materials, 38, (2000), 25-34

Mintova S., Hedlund J., Valtchev V., Schoeman B., and Sterte J., ZSM-5 films prepared from template free precursors,J. Mater. Chem., 1998, 8 (10), 2217 - 2221

Morigami Y., Konodo M., Abe J., Kita H., Okamoto K., The first large scale pervaporation plant using tubular type module with a zeolite NaA membrane, Separation and Purification Technology, 25, (2001), 251-260

Piera E., Salomon M., Coronas J., Menendez M., Santamaria J., Synthesis, characterisation and separation properties of a composite modernite/ ZSM-5/chabazite hydrophilic membrane, Journal of Membrane Science, 149, (1998), 99-114

Salomon M., Coronas J., Menendez M., Santamaria J., Synthesis of MTBE in the zeolite membrane reactors, Applied Catalysis: A: General, 200, (2000), 201-210

Sau Man Lai, Chi Po Ng, Rosa Martin-Aranda, King Lun Yeung, Knoevengel condensation reaction in zeolite membrane microreactor, Microporous and Mesoporous Materials, 66, (2003), 239-252

Seader and Henley, Separations process principals, John Wiley and Sons inc., (1998)

Sommer S., Melin T., Falconer J., Noble R., Transport of C_6 isomers through ZSM-5 zeolite membranes, Journal of Membrane Science 224, (2003), 51-67

Taylor R. and Krishna R., Multi-component mass transfer, Chemical engineering, John Wiley and Sons inc., 1993

Urtiaga A., Gorri E., Casado C., Ortiz I., Pervaporative dehydration of industrial solvents using a zeolite NaA commercial membrane, Separation and Purification Technology, 32, (2003), 207-213

Van Berge P., Van de Loosdrechta J., Barradas S., van der Kraanb S., Oxidation of cobalt based Fischer-Tropsch catalysts as a deactivation mechanism, Catalysis Today, 58, (2000), 321-334

Van Steen E., Schulz H., Polymerisation kinetics of the Fischer-Tropsch CO hydrogenation using iron and cobalt based catalysts, Applied Catalysis A: General, 186, (1999), 309-320

Wesselingh J. and Krishna R., Mass transfer in multicomponent mixtures, Amsterdam University press, (2000)

Xomeritakis G., Lai Z. and Tsapatsis M., Separation of Xylene Isomer vapours with oriented MFI membranes made by seed growth, Industrial Engineering Chemistry Research, 40, (2001), 544-552

Xu W., Dong J., Li J., and Wu F., A novel method for the preparation of zeolite ZSM-5, Journal of Chemical society and chemical communications (1990) 755-756

Part IV

Appendices

Appendix A

Derivation of FTS rate law

The rate law that describes the intrinsic rate of reaction is derived from a set of elementary gas-surface phase reactions include:

$$H_2 + 2^\bullet \rightleftharpoons 2H^\bullet \qquad K_H = \frac{\theta_H}{p_{H_2}^{0.5}\theta_\bullet} \tag{A.1}$$

$$CO{+}^\bullet \rightleftharpoons CO^\bullet \qquad K_{CO} = \frac{\theta_{CO}}{p_{CO}\theta_\bullet} \tag{A.2}$$

$$CO^\bullet{+}^\bullet \rightleftharpoons C^\bullet + O^\bullet \qquad K_C = \frac{\theta_{C^\bullet}\theta_{O^\bullet}}{\theta_{CO^\bullet}\theta_\bullet} \tag{A.3}$$

$$2H^\bullet + O^\bullet \rightleftharpoons H_2O + 3^\bullet \qquad K_{H_2O} = \frac{P_{H_2O}\theta_\bullet^3}{\theta_H^2\theta_O} \tag{A.4}$$

where $\bullet$ is the catalyst active site and yielding the FTS rate equation :

$$-r_{CO} = \frac{kK'\frac{p_{H_2}^{\frac{3}{2}}\cdot p_{CO}}{p_{H_2O}}}{\left(1 + K''\frac{p_{H_2}\cdot p_{CO}}{p_{H_2O}}\right)^2} \tag{A.5}$$

with K' and K"given by:

$$K' = K_H^3 K_{CO} K_C K_{H_2O} \tag{A.6}$$

$$K'' = K_H^2 K_{CO} K_C K_{H_2O} \tag{A.7}$$

Appendix B

Thermodynamics of Co oxidation

Figure B.1 shows the thermodynamic equilibrium of Co oxides under FTS conditions. The two oxide formation mechanisms are not thermodynamically favoured, however the combined Co, Al oxidation is thermodynamically favoured.

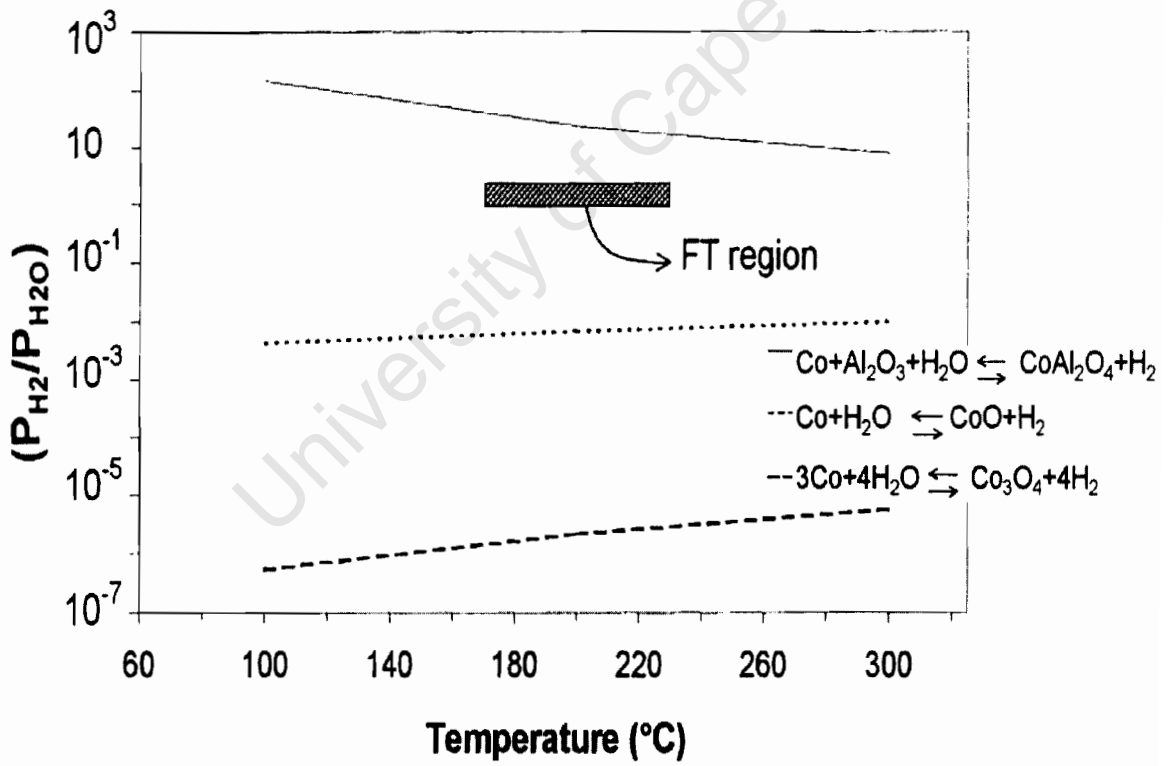

Figure B.1: Thermodynamic equilibrium constant as a function of temperature for oxidation reactions.

Appendix C

Calibration charts

Figures C.1, C.2, and C.3 show the calibration charts relating partial pressure of H_2, H_2O and nC_6 to the GC peak areas respectively. A known flowrate of H_2 and He were feed to H_2O and nC_6 saturators at 20°C and 1 bar and peak areas measured.

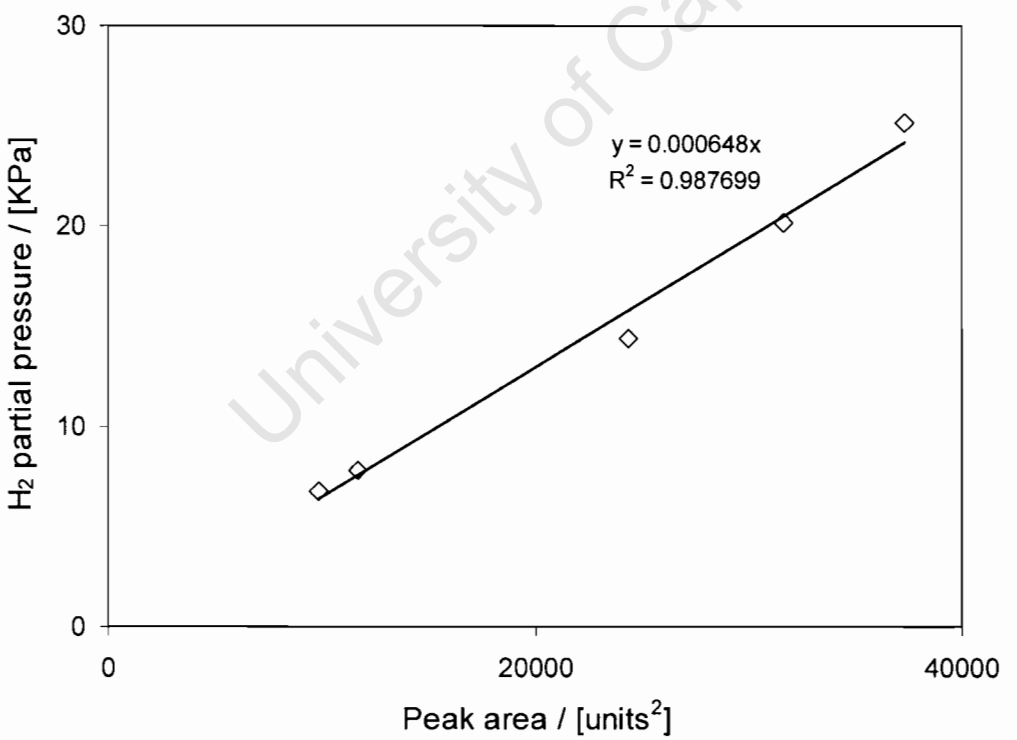

Figure C.1: Showing the H_2 calibration chart.

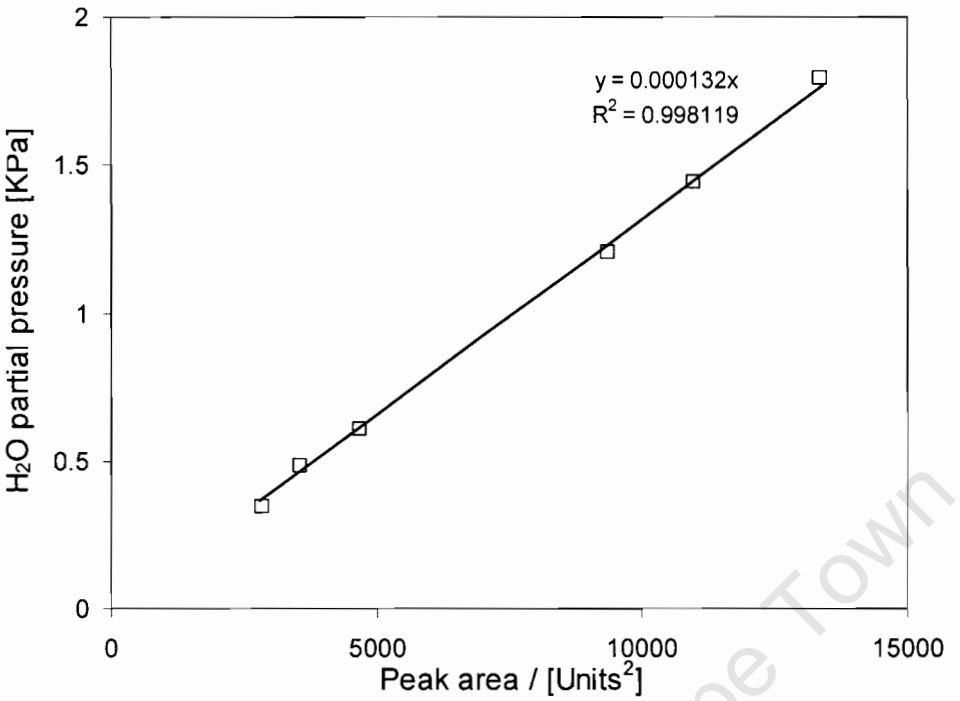

Figure C.2: Showing the H_2O calibration chart.

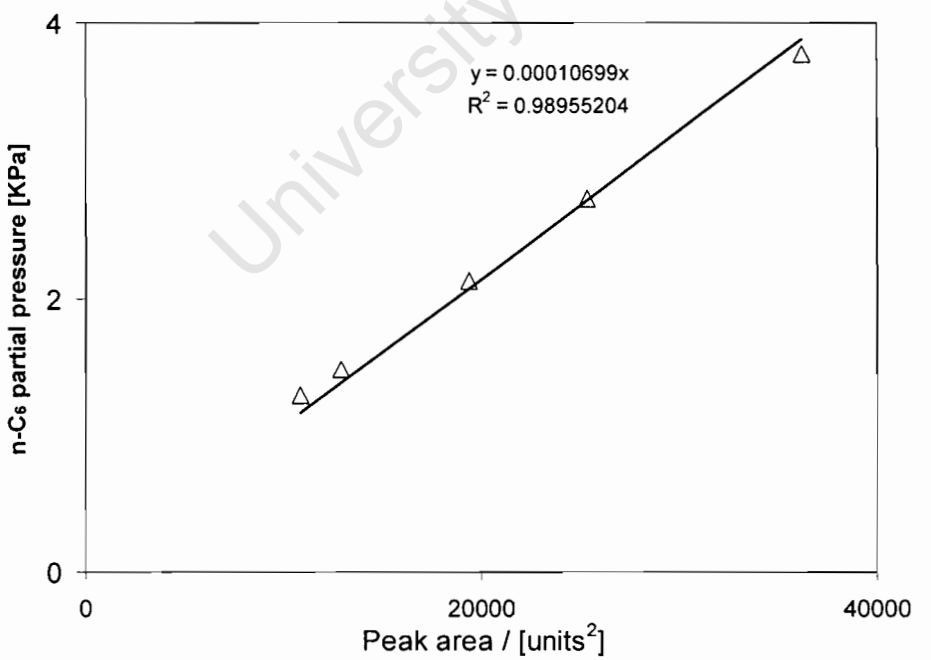

Figure C.3: Showing the nC_6 calibration chart.

Appendix D

Calculations and raw data

For single gas permeation flowrates were measured and these used to calculate the flux through the membrane as follows:

$$J_i = \frac{F_i}{A_{mem}} \tag{D.1}$$

$$\pi_i = \frac{F_i}{\Delta P_i} \tag{D.2}$$

For mixture separations peak area of each species in the permeate was measured and selectivity calculated from equation D.3:

$$\alpha_{i,j} = \frac{(PA_i/PA_j)_{permeate}}{(PA_i/PA_j)_{feed}} \tag{D.3}$$

Permeance was also calculated by relating peak areas to parial pressures using calibration charts in Appendix C. The flowrate of each species was then calculated and permeance calculated in the same way as single gas measurments:

$$p_i = PA_i a_i \tag{D.4}$$

a_i	partial pressure conversion factor (Pa)
A_{mem}	the surface area of the membrane exposed for permeation (m^2),
F_T	flowrate of permeate ($mlmin^{-1}$)
PA_i	the peak area of species i ($units^2$),

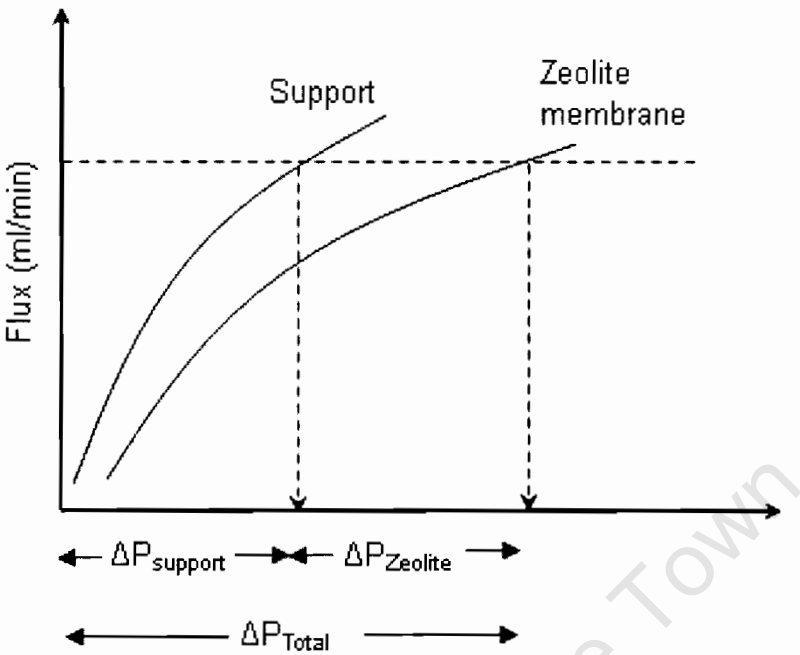

Figure D.1: Method used to calculate support contribution to pressure drop across the membrane

Table D.1: Maximum He permeance for Silicalite and ZSM-5 membranes in porosimetry

Membrane	S1	S2	S3	Z1	Z2	Z3
He_{max} (10^{-7} mol.m^{-2}.s^{-1}.Pa^{-1})	115	96	81	75	66	86

Table D.2: Contribution of viscous (gradient) and knudsen (intercept) flow for blank support

Species	H_2	He	CO_2	SF_6
Gradient	41.0	22.5	18.6	12.6
Intercept	0.0338	0.0134	0.0217	0.1200
Gradient/Intercept	1213	1679	857	105

Table D.3: Binary and ternary FID peak areas for S3

Binary			Tenary			
	Peaks Area			Peaks Area		
Temp [°C]	H_2	H_2O	Temp [°C]	H_2	H_2O	n-C_6
28	2146	5263	26	808	3805	7163
37	5439	5399	36	846	3928	11178
52	12882	6030	44	875	3529	11855
70	15394	6069	60	980	3561	13315
90	16030	6108	79	991	3618	14193
111	16647	6091	99	1593	3322	14590
133	17065	6184	120	3806	3712	15316
156	17288	6194	141	5704	4143	15692
177	17426	6103	162	7749	4232	15986
198	17482	6306	182	10476	4571	16001
218	17555	6255	202	13154	4651	16518
239	17572	6234	221	14874	5202	16465
259	17663	6282	241	15675	5613	16703
278	17711	6225	260	16135	6055	16636
298	17721	6203	279	16364	6018	16552
316	17809	6260	299	16465	6021	17404
335	17796	6191	318	16602	6032	17363
354	17776	6371	338	16673	6195	17326
366	17685	6332	357	16749	6089	17049
			377	16848	6154	17275

Table D.4: Binary and ternary FID peak areas for Z1

Binary			Ternary			
	Peaks			Peaks		
Temp	H_2	H_2O	Temp	H_2	H_2O	n-C_6
25	4238	4223	26	1112	3701	9337
26	4137	3823	36	1213	3679	11851
34	6279	3868	46	1398	3716	12832
45	12420	4852	75	2396	3715	12992
57	14439	5166	96	3549	3994	13600
70	15340	5723	113	6210	4187	14192
82	15757	5699	130	8569	4346	14545
95	16441	5714	147	10444	4711	14585
107	16521	6033	165	12185	5633	14743
121	16639	5875	183	13990	5742	15004
135	16708	5867	202	15562	5632	15225
149	16759	5847	220	16332	5725	15291
164	16797	5883	239	16780	5613	15241
178	16868	5936	259	16963	5730	15147
193	16938	6046	278	17118	5703	15608
209	16991	6099	298	17055	5950	15542
224	17074	6059	318	16965	6087	15206
240	17035	6139	338	16859	6093	15054
256	17076	6085	358	17015	6071	14954
273	17141	6071				
289	17150	6111				
306	17141	6066				
325	17301	6080				

Table D.5: Binary FID peak areas for S2

Binary			Ternary		
	Peaks			Peaks	
Temp	H2	H2O	Temp	H2	H2O
28	4724	4786	28	1405	3962
30	5310	4672	31	1428	4187
33	6745	4449	36	1410	4118
36	7993	4575	41	1431	3673
41	10979	5206	51	1480	3712
49	13231	5282	64	1596	3641
56	14331	5403	78	1810	3781
65	14859	5384	94	2373	3769
73	15093	5456	110	3667	4086
82	15589	5516	126	5501	3937
92	15956	5657	142	7305	4072
102	16497	5406	159	9259	4251
113	16836	5447	175	11409	4688
124	16995	5419	192	13632	5168
136	17047	5513	208	15203	5291
149	17113	5609	225	16100	5353
163	17638	5634	242	16516	5393
176	17802	5534	260	16788	5554
191	18003	5581	277	16884	5587
206	17848	5507	295	17029	5800
220	17793	5615	314	17325	5849
235	17892	5811	332	17408	5779
239	17932	5782	337	17482	5806

Table D.6: Binary FID peak areas for ZTF6

	Peaks	
Temp	H2	H2O
25	608	3620
30	729	3704
31	795	3935
37	868	3994
44	929	4170
52	982	4222
60	1051	4195
69	1119	4209
78	1189	4256
87	1255	4328
95	1316	4260
99	1338	4360
102	1353	4203
110	1416	4396
121	1476	4340
123	2391	4248
125	2621	4381
26	2401	4100

Table D.7: Raw porosimetry data

Membrane: S1

He [ml/min]	Sat He [ml/min]	Flow [ml/min]	Tcell °C	Tsat °C	P [kPag]	P/P0	Permeance [mol/s m^2 Pa]
500	0	333.30	20.80	16.80	101.40	0.0000	115.93
500	6	3.60	22.16	15.77	109.30	0.0089	1.16
450	14	2.80	22.80	16.17	112.50	0.0223	0.88
120	50	1.70	23.20	16.23	113.90	0.2144	0.53
0	50	0.95	23.50	16.28	115.30	0.7210	0.29
0	50	0.85	23.70	24.80	116.20	0.9999	0.26

Membrane: S2

He [ml/min]	Sat He [ml/min]	Flow [ml/min]	Tcell °C	Tsat °C	P [kPag]	P/P0	Permeance [mol/s m^2 Pa]
500	0	252.00	23.54	14.13	110.40	0.0000	80.51
500	6	1.90	23.74	14.46	110.10	0.0078	0.61
450	14	0.78	23.87	14.59	111.30	0.0198	0.25
120	50	0.52	24.05	14.78	111.60	0.1929	0.16
0	50	0.22	24.23	14.56	111.90	0.6441	0.07
0	50	0.15	24.29	25.25	112.00	0.9999	0.05

Membrane: S3

He [ml/min]	Sat He [ml/min]	Flow [ml/min]	Tcell °C	Tsat °C	P [kPag]	P/P0	Permeance [mol/s m^2 Pa]
500	0	277.00	24.90	15.11	101.90	0.0000	95.88
500	6	1.80	25.30	18.80	102.50	0.0089	0.62
450	14	1.40	25.90	21.90	103.00	0.0253	0.48
120	50	1.00	26.30	16.95	103.10	0.1937	0.34
0	50	0.63	26.60	16.65	103.20	0.6412	0.22
0	50	0.58	26.70	27.50	103.20	0.9999	0.20

Membrane: Z1

He [ml/min]	Sat He [ml/min]	Flow [ml/min]	Tcell °C	Tsat °C	P [kPag]	P/P0	Permeance [mol/s m^2 Pa]
500	0	214.00	22.09	14.34	100.80	0.0000	74.88
500	6	1.00	22.35	15.99	101.40	0.0089	0.35
450	14	0.71	22.59	16.42	101.90	0.0228	0.25
120	50	0.54	23.17	16.71	102.50	0.2195	0.19
0	50	0.40	23.35	16.69	102.90	0.7398	0.14
0	50	0.20	23.80	25.57	103.20	0.9999	0.07

Membrane: Z2

He [ml/min]	Sat He [ml/min]	Flow [ml/min]	Tcell °C	Tsat °C	P [kPag]	P/P0	Permeance [mol/s m^2 Pa]
500	0	207.00	23.15	15.40	111.50	0.0000	65.48
500	6	1.40	23.30	15.50	112.30	0.0083	0.44
450	14	1.20	23.40	15.60	112.60	0.0212	0.38
120	50	1.00	23.50	15.70	112.70	0.2064	0.31
0	50	0.88	23.70	15.60	113.10	0.6923	0.27
0	50	0.69	23.80	24.60	113.60	0.9999	0.21

Membrane: Z3

He [ml/min]	Sat He [ml/min]	Flow [ml/min]	Tcell °C	Tsat °C	P [kPag]	P/P0	Permeance [mol/s m^2 Pa]
500	0	243.00	23.13	18.02	100.20	0.0000	85.53
500	6	73.00	24.15	18.40	100.60	0.0092	25.59
450	14	71.00	24.65	18.58	100.90	0.0230	24.82
120	50	68.00	24.71	18.49	100.70	0.2228	23.82
0	50	52.20	24.70	18.20	84.90	0.7477	21.69
0	50	49.10	24.70	25.60	80.00	0.9999	21.65

Table D.8: Single gas flowrates for blank substrate as a function of temperature for trans membrane pressure drop=0.3 bar

	Flowrate (ml/min)			
Temperature (K)	H_2	He	CO_2	SF_6
298	852	470	316	227
323	771	438	276	217
373	679	371	215	167
473	512	315	161	137
573	449	280	126	110

Table D.9: Single gas flowrates for blank support as a function of trans membrane pressure drop at 25°C

	Flow rate (ml/min)			
ΔP (KPa)	H_2	He	SF_6	CO_2
100				746
90			924	694
80			812	641
70			655	568
60		981	560	470
50		848	451	360
40		626	382	277
38	1018			
35	883	510		
30	771	438	276	217
25	614	381		
20	434	299	174	149
15	316	187		
10	159	138	59	59

Table D.10: Single gas flowrates for S2 as a function of trans membrane pressure drop at 25°C

	Flow rate (ml/min)			
ΔP (KPa)	H_2	He	SF_6	CO_2
110		385	82	629
100	1005	366	78	562
90	917	343	74	537
80	801	305	68	485
70	661	256	63	439
60	564	223	54	354
50	433	181	46	318
40	324	150	39	272
30	244	103	27	179
20	146	61	20	104
10	46	25	7.2	51

Table D.11: Single gas flowrates for Z1 as a function of trans membrane pressure drop at 25°C

	Flow rate (ml/min)			
ΔP (KPa)	H_2	He	SF_6	CO_2
110	850	575	40	664
100	764	499	37	599
90	668	455	34	538
80	566	403	30	470
70	485	348	27	433
60	415	302	24	373
50	342	235	23	316
40	265	198	18	256
30	184	108	13	198
20	102	82	8.7	110
10	37	30	2.3	50

Table D.12: Assumed MS model parameters used so as to fit experimental data

Species	E_a^{sur}[J.mol^{-1}]	ΔH^{ads}[J.mol^{-1}]	$Đ_i$[m^2.s^{-1}]	b_i[Pa^{-1}]
H_2	22 000	14 000	4×10^{-11}	1.3×10^{-5}
H_2O	32 000	34 000	1×10^{-11}	6.7×10^{-3}
nC_6	5 000	10 000	4×10^{-12}	2.0×10^{-3}

Appendix E

Permeance at relative pressures

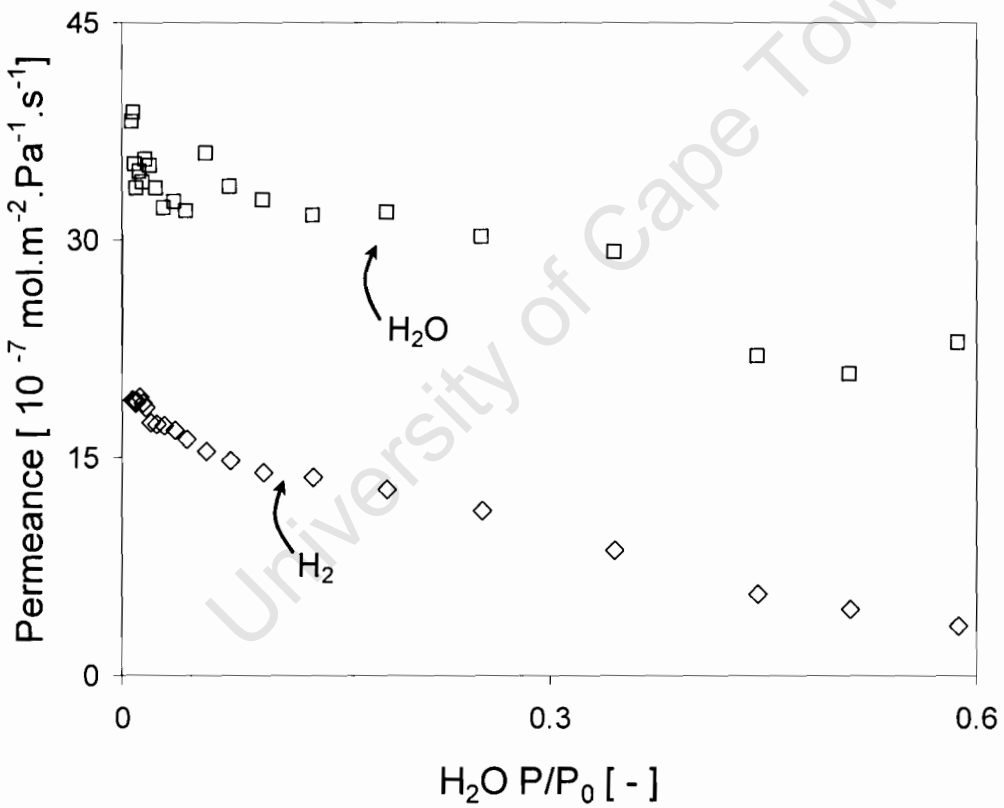

Figure E.1: Binary permeance of H_2 and H_2O as a function of relative partial pressure of H_2O for S3.

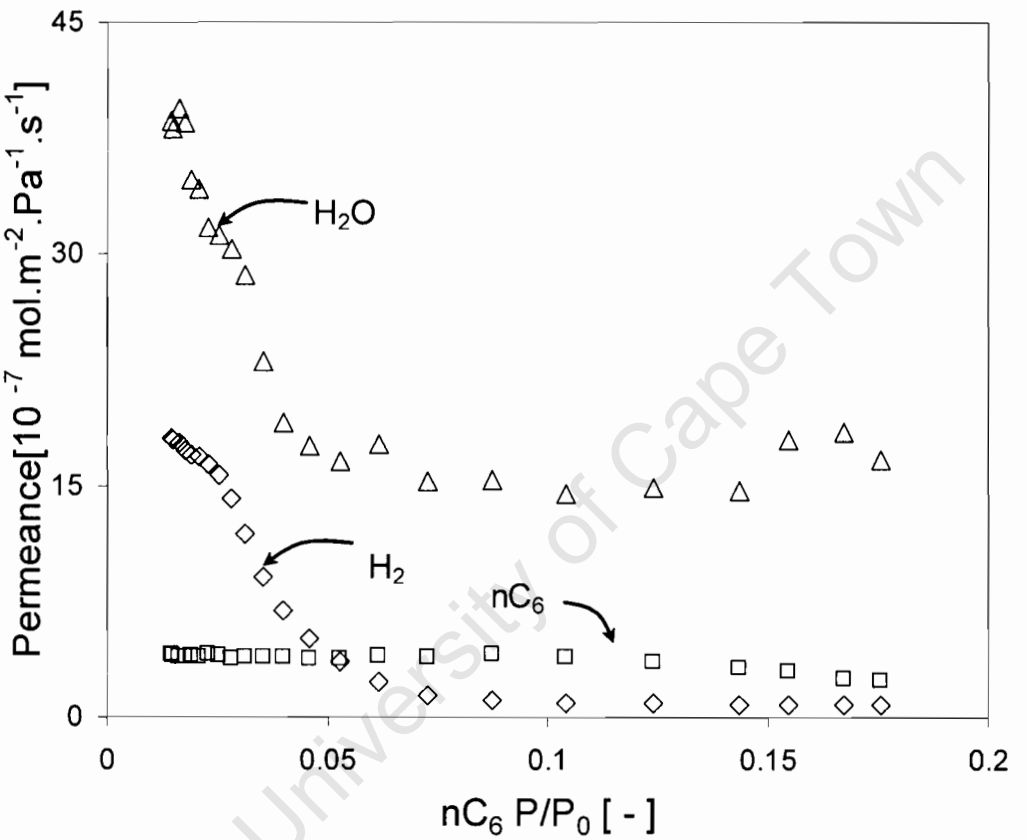

Figure E.2: Ternary permeance of H_2,H_2O and nC_6 as a function of relative partial pressure of nC_6 for S3.